An Improved Human Ventricular Cell Model for Investigation of Cardiac Arrhythmias under Hyperkalemic Conditions

Author: Jesús Carro Fernández

Directors: Esther Pueyo and José Félix Rodríguez

Master's Degree in
Biomedical Engineering

December, 2010
Academic Year: 2010-2011

Universidad Zaragoza
1542
Communications Technology Group
Group of Structural Mechanics and Material Modeling

An Improved Human Ventricular Cell Model for Investigation of Cardiac Arrhythmias under Hyperkalemic Conditions

Author: Jesús Carro Fernández

Directors: Esther Pueyo and José Félix Rodríguez

Master's Degree in
Biomedical Engineering

December, 2010
Academic Year: 2010-2011

Universidad Zaragoza
1542
Communications Technology Group
Group of Structural Mechanics and Material Modeling

To Débora.
To my family.

An Improved Human Ventricular Cell Model for Investigation of Cardiac Arrhythmias under Hyperkalemic Conditions

Abstract

The use of experiments for studying cardiac arrhythmias or the effect of drugs on cardiac electrophysiology is mostly limited to measurements obtained from electrograms (EGMs, measured on the heart surface) or, more often, electrocardiograms (ECGs, measured on the body surface). Despite the fact that many diagnostic and therapeutical decisions rely only upon interpretation of ECG patterns, the cellular and subcellular mechanisms underlying pathophysiological ECG changes remain mostly unclear. Among the different approaches aimed to connect the ECG with its underlying basis, multi-scale computational modeling of the heart arises as a powerful tool to understand cardiac functioning from the ionic to the whole organ level. With the increase in computational resources available to the scientific community, mathematical modeling and simulation of heart's electrical activity is becoming a fundamental tool to understand cardiac behavior.

In this study several modifications were introduced to a recently proposed action potential (AP) cell model so as to render it suitable for the study of ventricular arrhythmias. These modifications were based on new experimental data and in the results of several cellular arrhythmic risk biomarkers reported in the literature.

Five stimulation protocols were applied to the original and improved models of isolated cell, and a number of cellular arrhythmic risk biomarkers were computed. The stimulation protocol included a steady-state protocol, abrupt changes in cycle length (CL) protocol, S1S2 and dynamic restitution protocols, and concentration rate dependence protocol.

In addition, the behavior of the proposed model under hyperkalemic conditions was simulated in a one dimensional fiber by increasing the extracellular $[K^+]$, measuring the AP duration (APD), conduction velocity (CV) and effective refractory period (ERP) after steady-state conditions had been reached.

Our modifications led to: a) further improved AP triangulation ($78.1\ ms$); b) APD rate adaptation curves characterized by fast and slow time constants within physiological ranges ($10.1\ s$ and $105.9\ s$); c) maximum S1S2 restitution slope in accordance with experimental data ($S_{S1S2} = 1.0$).

Under hyperkalemia, our results showed that APD progressively decreased with the level of hyperkalemia, while ERP increased after a threshold in the extracellular $[K^+]$ was reached ($[K^+]_o = 6\ mM$). Conduction velocity decreased with hyperkalemia and the conduction was blocked above $[K^+]_o = 10.4\ mM$. Above $[K^+]_o = 9.8\,mM$, alternans appeared in the APD. These results suggest that the longer ERP values and the conduction block above $[K^+]_o = 10.4\,mM$ found in the central zone of acutely ischemic tissue as compared to the normal zone could create areas of block that could set a substrate for reentrant arrhythmias.

Mejora de un Modelo Celular de Ventrículo Humano para la Investigación de Arritmias Cardiacas bajo Condiciones de Hiperpotasemia

Resumen

La utilización de experimentos para el estudio de arritmias cardiacas o el efecto de medicamentos en la electrofisiología cardiaca está limitada principalmente a medidas obtenidas de los electrogramas (EGMs, medidos en la superficie del corazón) o, más habitualmente, electrocardiogramas (ECGs, medidos en la superfice del cuerpo). A pesar de que muchos diagnósticos y decisiones terapéuticas están fundadas solamente en la interpretación de los patrones de ECG, los mecanismos celulares y subcelulares subyacentes a cambios fisiopatológicos en el ECG, continúan no quedando claros en la mayoría de casos. Entre los diferentes acercamientos para conectar el ECG con los mecanismos subyacentes, el modelado computacional multiescala del corazón se plantea como una herramiente potente para entender el funcionamiento cardiaco, desde el nivel iónico al órgano completo. Con el incremento de los recursos computacionales disponibles para la comunidad científica, el modelado matemático y la simulación de la actividad eléctrica del corazón se está convirtiendo en una herramienta fundamental para comprender el comportamiento cardiaco.

En este estudio, varias modificaciones fueron introducidas a un modelo de potencial de acción (AP) propuesto recientemente, para hacerlo apto para el estudio de arritmias ventriculares. Estas modificaciones se basaron en nuevos datos experimentales y en el resultado de varios biomarcadores arrítmicos celulares presentados en la literatura.

Se aplicaron cinco protocolos de estimulación al modelo origninal y a la versión mejorada para calcular los diferentes biomarcadores de riesgo arrítmico. Los protocolos de estimulación incluían un protocolo de estado estático, un protocolo de cambios abruptos en el período de estimulación (CL), los protocolos de restitución S1S2 y dinámico, y un protocolo de depencencia de las concentraciones a la frecuencia cardiaca.

Además, se simuló el comportamiento del modelo propuesto bajo condiciones de hiperpotasemia en una fibra unidimensional mediante el incremento de la concentración extracelular de K^+, midiendo la duración del AP (APD), la velocidad de condución (CV) y el período refractario efectivo tras alcanzar condiciones de estado estable.

Estas modificaciones llevaron a: a) mejorar aún más la triangulación del APD ($78,1\ ms$); b) Caracterización del APD mediante una constante de tiempo rápida y una lenta dentro del rango fisológico ($10,1\ s$ y $105,9\ s$); c) máxima pendiente de la curva de restitución S1S2 en concordancia con los datos experimentales ($S_{S1S2} = 1,0$).

Bajo condiciones hiperpotasémicas, los resulatos mostraron que el APD decrece progresivamente con el nivel de hiperpotasemia, mientras que el ERP aumenta tras un umbral en la concentración extracelular de K^+ ($[K^+]_o = 6\ mM$). La CV disminuyó con hiperpotasemia y la conducción se bloqueó por encima de $[K^+]_o = 10,4\ mM$. Por encima de $[K^+]_o = 9,8\ mM$, aparecieron alternantes en el APD. Estos resultados sugieren que los altos valores de ERP y el bloqueo de conducción sobre $[K^+]_o = 10,4\ mM$ encontrado en la zona central de tegido isquémico agudo, puede crear un área de bloqueo que sea el substrato para un arrhitmia reentrante.

Index

Contents

List of Figures

List of Tables

Document

Chapter 1

Introduction

Cardiovascular disease (CVD) is the main cause of death in industrialised countries. More than 2 million people in the European Union (EU) and nearly 4.5 million people in all Europe die from CVD every year (European Heart Network 09), a number which is well above that of people dying from cancer, dementia and HIV/AIDS all together (World Health Organization 09). CVD is thus responsible for 42% of total deaths in the EU (38% of female, and 45% of male deaths). Spain, despite being one of the countries with the lowest rate of mortality due to CVD within Europe, is showing a tendency to a worst perspective, with a 2.1% increment per year in the number of such deaths.

1.1 Cardiac Arrhythmias

Among CVD, cardiac arrhythmias represent a common cause of mortality. Cardiac arrhythmias are conditions in which there is a failure in the normal rhythm of the heartbeat. Arrhythmias can be caused either by an abnormal formation of the electrical impulse, by abnormalities in the conduction of that impulse throughout the heart, or by both. There are different types of cardiac arrhythmias. The so-called re-entrant arrhythmias occur when a propagating impulse fails to die out after normal activation of the heart and persists to re-excite other regions that have already recovered excitability. Some arrhythmias of this type are dangerous and may have fatal consequences.

Frequently occurring re-entrant arrhythmias in the ventricles include monomorphic and polymorphic ventricular tachycardia (VT) and ventricular fibrillation (VF). Monomorphic VT and polymorphic VT (among which Torsades de Pointes) both lead to increased ventricular excitation and contraction rates and a decrease of cardiac output. In addition, both may destabilize into VF. VF leads to a further increase in excitation rate and a loss of coherence of ventricular contraction, which results in almost zero cardiac output. This will cause death to occur within minutes unless normal sinus rhythm is restored. In Europe sudden cardiac death (SCD) accounts for over 300,000 deaths per year, of which 75-80% are due to VF. VT and VF thus belong to the most dangerous cardiac arrhythmias.

1.2 Ischemia

Ischemia is a pathological condition in which the delivery of substrates, mainly oxygen, to the myocardium is reduced. This causes a progressive deterioration of the electrical activity in the injured region. Three are the main components of the cellular alterations under ischemia: hyperkalemia, acidosis and hypoxia (Dodama et al., 1984; Gilmour and Zipes, 1980; Kagiyama et al., 1982; Kishida et al., 1979; Senges et al., 1979; Vleugels et al., 1980).

Under hyperkalemia, potassium starts to pour out of ischemic myocardial cells causing a depolarization of the myocardium at rest, slowing conduction and decreasing excitability. Under these conditions, recovery of excitability is known to outlast repolarization, a phenomenon termed post-repolarization refractoriness.

Hypoxia causes a reduction in the ATP/ADP ratio than can slow down calcium pumps and exchangers (Tian and Ingwall, 1196), increasing intracellular sodium and calcium concentrations as well as activating ATP sensitive potasium channels ($I_{K_{ATP}}$ channels) (Carmeliet, 1999). Acidosis reduces the availability of sodium and calcium channels, reducing excitability and slowing conduction.

These abnormalities cause inhomogeneities of resting potential and dispersion in recovery of excitability in the tissue. In addition, these inhomogeneities set the stage for unidirectional block that can become the substrate for cardiac arrhythmias.

1.3 New Methods for Diagnosis and Treatment

Due to the high incidence of CVD in the European population, and among this of cardiac arrhythmias, the associated cost with it turns out to be huge. It is estimated that CVD costs the EU economy €192,000 million a year, and €7,000 million a year to the Spanish Government, thus becoming the main cause of disease burden (European Heart Network 09). Based on these numbers it is clear that industrialised countries, and in particular Europe and Spain, need to face the challenge of appropriately managing prevention, diagnosis and treatment of cardiac diseases but at affordable cost. It is in this context where computational tools may provide relevant capabilities to improve quality and efficiency of healthcare services.

Mathematical modeling and simulation of heart's electrical activity (so-called cardiac electrophysiology) and signal processing of bioelectrical signals provide an ideal framework where to join the information from clinical and experimental studies with the understanding of the mechanisms underlying them so as to produce tools able to test different hypothesis and predict potential abnormalities in heart's behavior. In a relatively near future it is not unlikely that those tools might even become to start being used in clinical practice as complementary instruments to help in the prevention of cardiac diseases and the improvement of their diagnosis and therapy.

1.4 Computational Modeling and Simulation

At present, clinical data is mostly limited to measurements obtained from electrograms (EGMs, measured on the heart surface) or, more often, electrocardiograms (ECGs, measured on the body surface). The main reason behind the extensive use of the ECG signal in the clinics can be found in the fact that, in addition to being a non-invasive procedure, is simple and of low-cost. Despite the fact that many diagnostic and therapeutical decisions rely only upon interpretation of ECG patterns, the cellular and subcellular mechanisms underlying pathophysiological ECG changes remain mostly unclear. Among the different approaches aimed to connect the ECG with its underlying basis, multi-scale computational modeling of the heart arises as a powerful tool to understand cardiac functioning from the ionic to the whole organ level.

There are a number of important reasons that support the use of cardiac models to explain ECG-derived outcomes. First, modeling represents an alternative to experimental investigation, which is pretty much limited by ethical considerations, particularly when dealing with human hearts. Animal experimentation on other species, such as guinea pigs, rabbits or pigs, turns out to be more feasible, but corresponding results are not always easily transferable to humans, due to differences in key aspects such as heart size, heart rate, or duration and shape of the action potential (AP, representative of the electrical activity of a cell) (ten Tusscher et al., 2004). Another advantage of modeling is that it offers the possibility to test hypothesis or investigate conditions that are not easily reproducible in experiments, as it is the case with the study of three-dimensional phenomena, where experimental recording techniques offer limited possibilities due to poor spatial resolution, poor depth resolution, or applicability only to wedge preparations (ten Tusscher, 2004). Finally, computer models are of great importance in fields such as drug testing, where the use of simulations can help to detect adverse properties of compounds before their commercialization, and thus reduce the cost of bringing a new drug to the market.

Computational modeling of the heart has experienced a great development during the last five decades. In 1960 Noble formulated the first electrophysiological model for cardiac myocytes (Noble, 1960), and since

then more complex models of cellular electrical activity have been proposed for different species and regions of the heart (Courtemanche et al., 1998; Grandi et al., 2010; Luo and Rudy, 1991, 1994; Maleckar et al., 2009; Noble et al., 1998; ten Tusscher and Panfilov, 2006). Additional modeling of the communication between neighbouring cells makes it possible to extend those cell models and convert them into tissue or even whole organ models. The electrical properties of the myocardium are generally described by the bidomain equations, a set of coupled parabolic and elliptic partial differential equations (PDEs) that represents the tissue as two separate, distinct continua - one intracellular and the other extracellular. The intracellular and the extracellular media are connected via the cell membrane, and thus the two PDEs are coupled at each point in space through a set of non-linear ordinary differential equations (ODEs), which describe the ionic transport across the cell membrane. In some cases, the monodomain representation of cardiac activity is used, which involves solving a single parabolic PDE, by assuming either that the extracellular potentials are negligible, or that the anisotropy ratios are equal in the intracellular and the extracellular domains (Bernabeu et al., 2009).

1.5 Human Ventricular Cell Models

In the last years some mathematical models of electrical and ionic homeostasis in human ventricular myocytes have been proposed. One of the most extensively used models is the one proposed by ten Tusscher and Panfilov (ten Tusscher and Panfilov, 2006) (TP06), which is an improved version of the model described in (ten Tusscher et al., 2004) (TNNP04), where the calcium dynamics, the slow delayed rectifier current (I_{Ks}) and the L-type calcium current (I_{CaL}) were reformulated. The major advantage of the TP06 model is that it accurately reproduces the behavior of the AP duration restitution curve (see Section 2 for more information about this). Other relevant model for human ventricular cells was described in the paper by Iyer et al. (Iyer et al., 2004). In this model the main ionic currents are described using Markovian chains, the reason for which the model becomes very complex, having more than 60 state variables. Recently, a new model of human ventricular AP has been proposed by Grandi et al. (Grandi et al., 2010) (GPB), which improves the response to frequency changes and has a better performance against current blocks with respect to the TP06 model.

1.6 This Work

Despite the fact that the human ventricular AP models currently available in the literature are able to reproduce certain electrophysiological properties, they fail in representing other relevant aspects, as will be later described. In order to obtain a model suitable for the study of cardiac arrhythmias, in this study we have worked on building a new human ventricular AP model based on the analysis of well-known arrhythmic risk biomarkers. For that, we have used the GPB model as a starting point, and we have modified it by accounting for recent experimental measurements of potassium currents (Fink et al., 2008) and by introducing fast and slow voltage-dependent inactivation gates for the L-type calcium current (ten Tusscher and Panfilov, 2006).

All the modifications were made with the aim of improving the model performance on several arrhythmic risk biomarkers (see Chapter 2). The proposed model, herein denoted by CRLP, has been tested against the GPB and TP06 models by applying four stimulation protocols and computing twelve cellular arrhythmic risk biomarkers following the methodology proposed in (Romero et al., 2009). The results show that the introduced modifications have brought most biomarkers into the physiological range, and considerably improved others with respect to the GPB and TP06 models of AP.

The proposed model has also been tested under hyperkalemic conditions to evaluate the feasibility of using this model for studying the acute regional ischemic heart.

This document is structured in four chapters, each one with the following contents:

- Chapter 2 introduces the importance of using arhythmic risk biomarkers to develop models and describes each of the arrhythmic risk biomarkers used in the evaluation of the model and how they are computed.

- Chapter 3 establishes the basis for the development of the new CRLP model and describes the modifications introduced to the GPB model to render it more suitable for the study of cardiac arrhythmias.
- Chapter 4 describes the simulation tests conducted to evaluate model's performance and presents the corresponding results.
- Chapter 5 presents the discussion and the conclusions of the study.

In addition, other contents can be found in the appendices to the main document:

- Appendix A: Description of the CRLP human ventricular cell model.
- Appendix B: Contributions of the study to international conferences.
- Appendix C: Compilation of the acronyms used in the document.

Chapter 2

Biomarkers of arrhythmic risk

Arrhythmic risk biomakers are commonly used to predict drug cardioxicity in the development process of a new pharmacological compound. In a study developed by Romero et al. (Romero et al., 2009) an evaluation of how the principal ionic currents of a human ventricular cell model influence different biomarkers was presented. Despite these evidences, the traditional way of developing a cellular model is based on isolated measurements on cells (i.e., individual ionic currents or intracellular concentrations). The exclusive use of current measurements leads to many uncertainties, as it only provides information about the behavior of each current, but not about the contribution of each current to the global cellular behavior.

The main goal of this study is to propose a new methodology for the development of ionic cell models that joins the two types of approaches described above for model development. Specifically, in this study biomarkers of arrhythmic risk were used to drive the modifications of the model. While the formulation of individual currents was based on specific measurements, model parameters were adjusted based on different biomarkers that must remain within a physiological range. This allowed the proposed model to provide results in better concordance with experimental data.

In the following sections, the main cellular arrhythmic risk biomarkers are presented, and the protocols used to measured them are described.

2.1 Selected Biomarkers

In this study, a number of arrhythmic risk biomarkers proposed in the literature were selected to be used for model evaluation purposes, following the methodology described in (Romero et al., 2009):

- **APD:** The AP duration (APD) is considered the main preclinical biomarker of drug cardiotoxicity becasuse of its link to long QT syndrome (Hondeghem et al., 2001; Volders et al., 2000). Unless otherwise specified, APD is used to denote AP duration at 90% repolarization.
- **Triangulation:** This biomarker represents the shape of the end of the AP, calculated as the difference between the APD at 50% and 90% of the repolarization (Figure 2.1.a). Low triangulation values are indicative of square APs, while high values indicate triangular APs. It has been proposed as a predictor of serious proarrhythmia in (Hondeghem et al., 2001).
- **Systolic and diastolic $[Ca^{2+}]_i$ levels :** The calcium dynamics at different frequencies has been reported as a risk biomarker in (Bers and Despa, 2006; Pieske et al., 1999). These biomarkers evaluate the diastolic (calcium level at rest) and the systolic (calcium level at peak) values for different frequencies (Figure 2.1.b).
- **Time constants of the APD adaptation to abrupt changes in cycle length (CL):** The adaptation to abrupt changes in CL was proposed as an arrhythmic risk biomarker in (Pueyo et al., 2004). In (Pueyo et al., 2010) the APD adaptation to abrupt changes in CL was fitted by two exponentials with time constants τ_{fast} and τ_{slow} (Figure 2.1.c). These time constants were reported as cellular arrhythmic risk biomarkers.

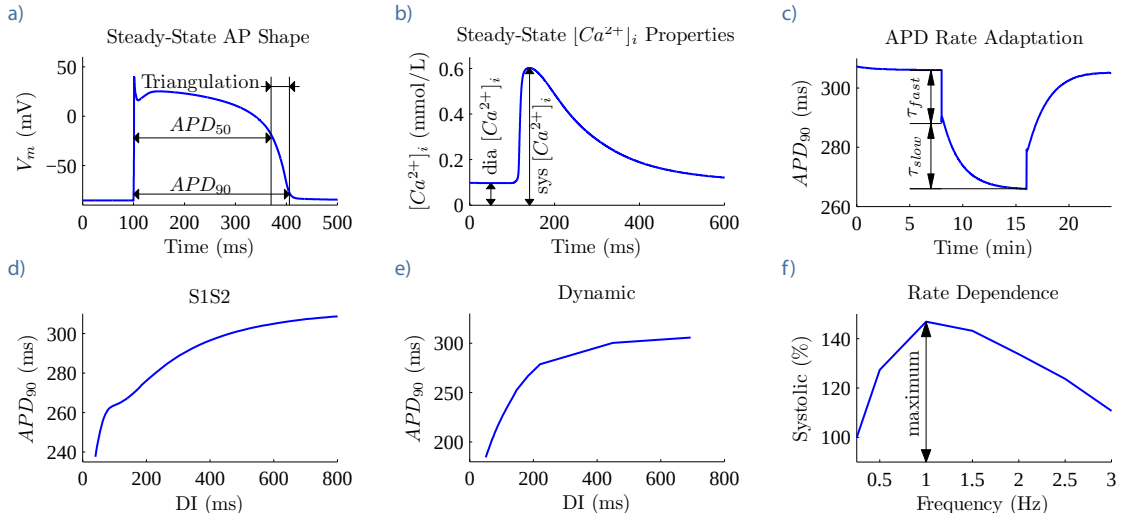

Figure 2.1. Graphical description of the biomarkers of arrhythmic risk used in this study: a) steady-state AP properties; b) steady-state $[Ca^{2+}]_i$; c) APD adaptation to abrupt changes in CL (from 1,000 ms to 600 ms and again to 1,000 ms); d) APDR curve computed using the S1S2 protocol; e) APDR curve computed using the dynamic procol; f) rate dependence of systolic concentrations.

- **Maximum slope of the APDR curves:** The maximum slope of the APD restitution (APDR) curve (Figures 2.1.d-e) was suggested as a risk biomarker in (Nolasco and Dahlen, 1968; Weiss et al., 2006). The APDR curve describes the relationship between the APD and the diastolic interval (DI), and in this study it has been evaluated using the S1S2 and the dynamic protocols (see Section 2.2).
- **Rate dependence of Na^+ and Ca^2+ concentrations:** The importance of intracellular sodium concentration ($[Na^+]_i$) and intracellular calcium concentration ($[Ca^{2+}]_i$) in arrhythmogenesis has been reported in (Levi et al., 1997; Murphy and Eisner, 2009).

2.2 Stimulation Protocols for Biomarkers Evaluation

Five stimulation protocols were applied to evaluate the risk bimoarkers presented in section 2.1. In all the cases, cells were stimulated with square transmembrane current pulses of 1-ms duration and twice the diastolic threshold at CL of 1,000 ms:

- **Steady-state protocol:** This protocol consists in the application of a train of 3,000 pulses to stabilize the cellular model. Simulations were carried out using two different CL values (1,000 and 2,000 ms). The evaluated biomarkers were: AP at 1 Hz, Triangulation at 1 Hz, Systolic $[Ca^{2+}]_i$ at 0.5 and 1 Hz, and Diastolic $[Ca^{2+}]_i$ at 0.5 and 1 Hz.
- **Abrupt changes in cycle length protocol:** The cell was stimulated with a CL of 1,000 ms for 8 minutes, then with a CL of 600 ms for additional 8 minutes and finally with a CL of 1,000 ms during 8 minutes (Figure 2.1). The dynamics of the first abrupt CL change were fitted by two exponentials with time constants τ_{fast} and τ_{slow}. The APD adaptation dynamics after the second abrupt CL change provided very similar results to those obtained for the first CL change, in accordance with (Pueyo et al., 2010; Romero et al., 2009), and are not reported.
- **S1S2 protocol:** This protocol consists of a train of 10 square current pulses at a CL of 1,000 ms followed by an extra stimulus applied at coupling intervals (CI) ranging from 1,000 to 250 ms. The S1S2

restitution curve was obtained by ploting the APD corresponding to the extrastimulus versus the previous diastolic interval (DI) for each of the values (Figure 2.1.d).

- **Dynamic protocol:** This protocol consists of 100 cycles applied at different CL values ranging from 1,000 to 50 ms. In this study the APDR curve was obtained by ploting the steady-state APD (corresponding to the 100^{th} stimulus of each CL) versus the corresponding steady-state DI (Figure 2.1.e).
- **Rate dependence protocol:** The systolic values of both $[Na^{+}]_i$ and $[Ca^{2+}]_i$ concentrations were measured at different frequencies (0.25, 0.5, 1, 1.5, 2, 2.5 and 3 Hz) and normalized to the level of the minimum frequency. For each frequency, the cell was stimulated during 10 minutes to reach steady-state. The maximum normalized concentration value was computed and used as a biomarker (Figure 2.1.f).

Chapter 3

Model Development

3.1 Modeling of electrical activity in cell and tissue

In general, the cell membrane is modeled as a capacitor connected in parallel with variable resistances and batteries representing the different ionic currents and pumps (Figure 3.1). Mathematically it can be expressed as:

$$C_m \frac{\mathrm{d}V_m}{\mathrm{d}t} = -\left(I_{ion} - I_{stim}\right),$$

where V_m represents the membrane potential, t denotes time, I_{ion} is the sum of all transmembrane ionic currents, I_{stim} is the externally applied stimulus current, and C_m is the cell capacitance per unit surface area.

In the case of simulating electrical propagation in a 1-D fiber, a parabolic reaction diffusion equation is used to describe the electrical activity of coupled cells:

$$C_m \frac{\partial V_m}{\partial t} = -\left(I_{ion} - I_{stim}\right) + \frac{\partial}{\partial x}\left(\sigma \frac{\partial V}{\partial x}\right),$$

where σ is the conductivity of the tissue and x is the coordinate along the fiber.

3.2 The available GPB Model

In the original GPB model, the total I_{ion} current is given by:

$$I_{ion} = I_{Na_{tot}} + I_{Cl_{tot}} + I_{Ca_{tot}} + I_{K_{tot}},$$

where each of the individual currents denote the current generated by the pass of the ions of sodium, chlorine, calcium and potassium, respectively, through the cell membrane.

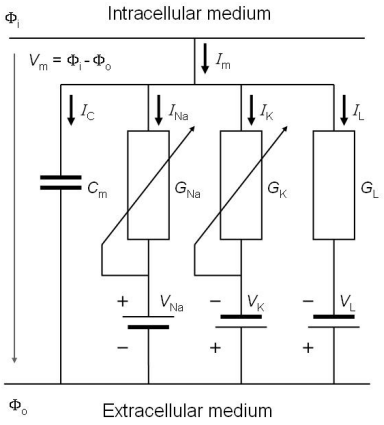

Figure 3.1. An electric circuit representation of a membrane patch. In this diagram, V_{Na}, V_K, and V_L represent the absolute values of the respective electromotive forces and the signs indicate their directions when the extracellular medium has a normal composition (high Na^+ and Cl^+, and low K^+ concentrations). Graphic from (Plonsey and Malmivuo, 1995).

3.2.1 Sodium current

The sodium current is divided into two components, which correspond to the parts of the membrane where the current is generated: subsarcolemmal or junctional zone. Both of them are composed by the same subcurrents:

$$I_{Na_{tot_{junc}}} = I_{Na_{junc}} + I_{NaBk_{junc}} + 3 \cdot I_{ncx_{junc}} + 3 \cdot I_{Na,K_{junc}} + I_{CaNa_{junc}}$$
$$I_{Na_{tot_{sl}}} = I_{Na_{sl}} + I_{NaBk_{sl}} + 3 \cdot I_{ncx_{sl}} + 3 \cdot I_{Na,K_{sl}} + I_{CaNa_{sl}}$$
$$I_{Na_{tot}} = I_{Na_{tot_{junc}}} + I_{Na_{tot_{sl}}}$$

where I_{Na} is the fast sodium current, I_{NaBk} is the background sodium current, I_{ncx} is the current of the sodium-calcium exchanger, $I_{Na,K}$ is the current of the sodium-potassium pump, and I_{CaNa} is the sodium current through the L-type calcium channels.

3.2.2 Chlorine current

The chlorine current, which is not present in the TP06 model, is described in the GPB model by:

$$I_{Cl_{tot}} = I_{ClCa} + I_{ClBk}$$

where I_{ClCa} is the calcium-activated chlorine current, and I_{ClBk} is the background chlorine current.

3.2.3 Calcium current

The calcium current, as the sodium current, has two components, junctional and subsarcolemal:

$$I_{Ca_{tot_{junc}}} = I_{Ca_{junc}} + I_{CaBk_{junc}} + I_{pCa_{junc}} - 2 \cdot I_{ncx_{junc}}$$
$$I_{Ca_{tot_{sl}}} = I_{Ca_{sl}} + I_{CaBk_{sl}} + I_{pCa_{sl}} - 2 \cdot I_{ncx_{sl}}$$
$$I_{Ca_{tot}} = I_{Ca_{tot_{junc}}} + I_{Ca_{tot_{sl}}}$$

where I_{Ca} is the calcium current through the L-type calcium channels, I_{CaBk} is the background calcium current, I_{pCa} is the sarcolemmal calcium pump current, and I_{ncx} is the current of the sodium-calcium exchanger.

3.2.4 Potassium Current

Finally, the potassium current is defined as follows:

$$I_{K_{tot}} = I_{to} + I_{Kr} + I_{Ks} + I_{K1} - 2 \cdot I_{Na,K} + I_{CaK} + I_{Kp}$$

where I_{to} is the transient outward potassium current, I_{Kr} is the rapidly activating potassium current, I_{Ks} is the slowly activating potassium current, I_{K1} is the inward rectifier potassium current, $I_{Na,K}$ is the current of the sodium-potassium pump, I_{CaK} is the potassium current through the L-type calcium channels, and I_{Kp} is the plateau potassium current.

3.3 The Proposed CRLP Model

Taking the GPB model as a starting point and with the aim of obtaining a better model to investigate cardiac arrhythmias, two ionic currents (I_{CaL} and I_{K1}) were reformulated and some model parameters of the GPB model were redefined. In the following sections, all these modifications are presented as well as the data and criteria they were based on.

3.3.1 L-Type Calcium Current (I_{CaL})

In order to obtain an APD adaptation response to abrupt changes in CL in better concordance with experimental data, the L-type calcium current was reformulated. The voltage-dependent inactivation gate f of the GPB model was replaced with the product of a fast, f, and a slow, f_2, inactivation gates, as in (ten Tusscher and Panfilov, 2006). The new equations for the L-type current in our CRLP model are as follows:

$$\begin{aligned}
I_{Ca_{junc}} &= F_{junc_{Ca_L}} \cdot \bar{I}_{Ca_j} \cdot d \cdot f \cdot f_2 \cdot \left(1 - f_{Ca_{B_j}}\right) \\
I_{Ca_{sl}} &= F_{sl_{Ca_L}} \cdot \bar{I}_{Ca_{sl}} \cdot d \cdot f \cdot f_2 \cdot \left(1 - f_{Ca_{B_{sl}}}\right) \\
I_{Ca_{Na_{junc}}} &= F_{junc_{Ca_L}} \cdot \bar{I}_{Na_j} \cdot d \cdot f \cdot f_2 \cdot \left(1 - f_{Ca_{B_j}}\right) \\
I_{Ca_{Na_{sl}}} &= F_{sl_{Ca_L}} \cdot \bar{I}_{Na_{sl}} \cdot d \cdot f \cdot f_2 \cdot \left(1 - f_{Ca_{B_{sl}}}\right) \\
I_{Ca_K} &= \bar{I}_K \cdot d \cdot f \cdot f_2 \cdot \left(F_{junc_{Ca_L}} \cdot \left(1 - f_{Ca_{B_j}}\right) + F_{sl_{Ca_L}} \cdot \left(1 - f_{Ca_{B_{sl}}}\right)\right)
\end{aligned}$$

Additionally, the value of the opening rate α_{f_2}, associated with f_2, was modified based on available experimental data (Figures 3.2a-b). Figure 3.2.a depicts τ_f and τ_{f_2} along with experimental data (Benitah et al., 1992; Beuckelmann et al., 1991; Li et al., 1999; Mewes and Ravens, 1994; Sun et al., 1997). The equations that describe f and f_2, including the new definition of α_{f_2}, are the following:

$$\begin{aligned}
f_{ss} &= \frac{1}{1 + e^{\frac{V_m + 20}{7}}} \\
\alpha_f &= 1102.5 \cdot e^{-\left(\frac{V_m + 27}{15}\right)^2} \\
\beta_f &= \frac{200}{1 + e^{\frac{13 - V_m}{10}}} \\
\gamma_f &= \frac{180}{1 + e^{\frac{V_m + 30}{10}}} + 20 \\
\tau_f &= \alpha_f + \beta_f + \gamma_f \\
\frac{\mathrm{d}f}{\mathrm{d}t} &= \frac{f_{ss} - f}{\tau_f}
\end{aligned}$$

$$
\begin{aligned}
f_{2_{ss}} &= \frac{0.67}{1+e^{\frac{V_m+35}{7}}} + 0.33 \\
\alpha_{f_2} &= 300 \cdot e^{\frac{-(V_m+25)^2}{170}} \\
\beta_{f_2} &= \frac{31}{1+e^{\frac{25-V_m}{10}}} \\
\gamma_{f_2} &= \frac{16}{1+e^{\frac{V_m+30}{10}}} \\
\tau_{f_2} &= \alpha_{f_2} + \beta_{f_2} + \gamma_{f_2} \\
\frac{\mathrm{d}f_2}{\mathrm{d}t} &= \frac{f_{2_{ss}} - f_2}{\tau_{f_2}}
\end{aligned}
$$

Additional modifications to the L-type calcium current include redefinition of the time constant τ_d of the activation gate d, which was replaced with the description given in (ten Tusscher and Panfilov, 2006). The equations for the activation gate d of the L-type calcium current in the CRLP model are:

$$
\begin{aligned}
d_{ss} &= \frac{1}{1+e^{\frac{-(V_m+5)}{6}}} \\
\alpha_d &= \frac{1.4}{1+e^{\frac{-35-V_m}{13}}} + 0.25 \\
\beta_d &= \frac{1.4}{1+e^{\frac{V_m+5}{5}}} \\
\gamma_d &= \frac{1}{1+e^{\frac{50-V_m}{20}}} \\
\tau_d &= \alpha_d \cdot \beta_d + \gamma_d \\
\frac{\mathrm{d}d}{\mathrm{d}t} &= \frac{d_{ss} - d}{\tau_d}
\end{aligned}
$$

The calcium-dependent inactivation gates ($f_{Ca_{B_j}}$ and $f_{Ca_{B_{sl}}}$) definitions were taken as in the GPB model:

$$
\begin{aligned}
\frac{\mathrm{d}f_{Ca_{B_j}}}{\mathrm{d}t} &= 1.7 \cdot Ca_j \cdot \left(1 - f_{Ca_{B_j}}\right) - 11.9 \cdot 10^{-3} \cdot f_{Ca_{B_j}} \\
\frac{\mathrm{d}f_{Ca_{B_{sl}}}}{\mathrm{d}t} &= 1.7 \cdot Ca_{sl} \cdot \left(1 - f_{Ca_{B_{sl}}}\right) - 11.9 \cdot 10^{-3} \cdot f_{Ca_{B_{sl}}}
\end{aligned}
$$

The relative permeabilities of the L-type calcium channels were adjusted to:

$$
\begin{aligned}
p_{Ca} &= 1.9887 \cdot 10^{-4}\, cm/s \\
p_K &= 5.4675 \cdot 10^{-8}\, cm/s \\
p_{Na} &= 3.0375 \cdot 10^{-9}\, cm/s
\end{aligned}
$$

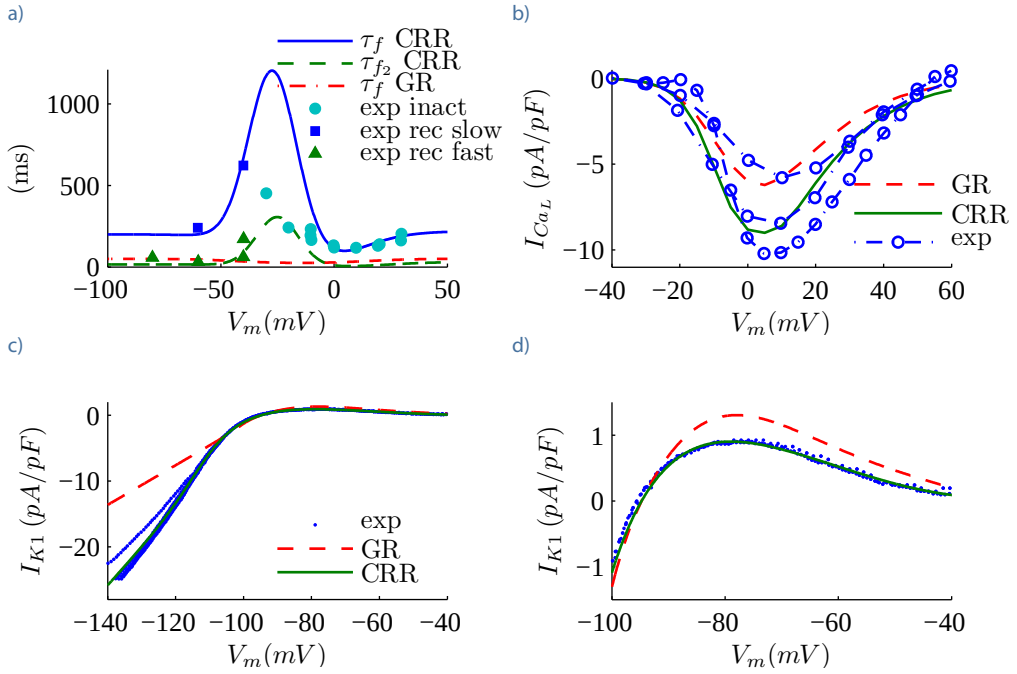

Figure 3.2. Current characteristics in simulations and experiments: a) I_{CaL} inactivation time constants as function of V_m; b) I_{CaL} current density versus voltage; c) maximum I_{K1} versus voltage and experimental data. $[K^+]_i = 138\ mM$ and $[K^+]_o = 4\ mM$; d) Detail of c. Blue dots and markers: experimental data.

$$\bar{I}_{Ca_j} = \frac{p_{Ca} \cdot V_m \cdot Frdy \cdot FoRT \cdot \left(Ca_j \cdot e^{2 \cdot V_m \cdot FoRT} - Ca_o\right)}{e^{2 \cdot V_m \cdot FoRT} - 1}$$

$$\bar{I}_{Ca_{sl}} = \frac{p_{Ca} \cdot V_m \cdot Frdy \cdot FoRT \cdot \left(Ca_{sl} \cdot e^{2 \cdot V_m \cdot FoRT} - Ca_o\right)}{e^{2 \cdot V_m \cdot FoRT} - 1}$$

$$\bar{I}_{Na_j} = \frac{p_{Na} \cdot V_m \cdot Frdy \cdot FoRT \cdot \left(Na_j \cdot e^{V_m \cdot FoRT} - Na_o\right)}{e^{V_m \cdot FoRT} - 1}$$

$$\bar{I}_{Na_{sl}} = \frac{p_{Na} \cdot V_m \cdot Frdy \cdot FoRT \cdot \left(Na_{sl} \cdot e^{V_m \cdot FoRT} - Na_o\right)}{e^{V_m \cdot FoRT} - 1}$$

$$\bar{I}_K = \frac{p_K \cdot V_m \cdot Frdy \cdot FoRT \cdot \left(K_i \cdot e^{V_m \cdot FoRT} - K_o\right)}{e^{V_m \cdot FoRT} - 1}$$

The results obtained with the new definition of the I_{CaL} current were compared against experimental data and against the results derived from the original definition of I_{CaL} in the GPB model. These results are presented in Figure 3.2.b. Experimental data is from (Li et al., 1999; Magyar et al., 2000; Pelzmann et al., 1998).

3.3.2 Inward Rectifier K Current (I_{K1})

The I_{K1} current was readjusted based on experimental data from (Fink et al., 2008). In the CRLP model, the I_{K1} current is formulated as follows:

$$a_{K1} = \frac{4.094}{1.0 + e^{0.1217 \cdot (V_m - E_K - 49.934)}}$$

$$b_{K1} = \frac{15.720 \cdot e^{0.0674 \cdot (V_m - E_K - 3.257)} + e^{0.0618 \cdot (V_m - E_K - 594.31)}}{1.0 + e^{-0.1629 \cdot (V_m - E_K + 14.207)}}$$

$$K1_{ss} = \frac{a_{K1}}{a_{K1} + b_{K1}}$$

$$I_{K1} = 0.5715 \cdot \sqrt{\frac{[K^+]_o}{5.4}} \cdot K1_{ss} \cdot (V_m - E_K)$$

where $[K^+]_o$ denotes the extracellular K^+ concentration, and E_K is the K^+ reversal potential. Figure 3.2.c shows the modified I_{K1} compared against the experimental data from (Fink et al., 2008) and I_{K1} from the GPB model. Note that Figure 3.2.c is a detail of Figure 3.2.c.

3.3.3 Na/K Pump Current ($I_{Na,K}$)

In order to improve the APD adaptation response to abrupt changes in CL, maximal $I_{Na,K}$ conductance was reduced by 45% with respect to the GPB model.

3.3.4 $[K^+]_i$ and G_{Na}

A more physiological value for $[K^+]_i$ of $138\ mM$ was used in our model. Considering this value for $[K^+]_i$ and in order to get physiological values for the maximal upstroke velocity in tissue, dV/dt, the maximum conductance of the sodium current, G_{Na}, was reduced to $18.86\ mS/\mu F$.

Chapter 4

Results

4.1 Conducted Simulations

Our proposed CRLP model was tested against the arrhythmic risk biomarkers described in chapter 2 and the results were compared against those obtained using the previously published TP06 and GPB human ventricular cell models. Also, in order to test the model in the same situations described in (Grandi et al., 2010), current blocks were simulated as reported in (Grandi et al., 2010). Finally, the behavior of the model under hyperkalemic conditions was simulated in a one-dimensional fiber, and conduction velocity (CV), APD and effective refractory period (ERP) were measured.

Cells were stimulated with square transmembrane current pulses twice the diastolic threshold and 1-ms duration. Forward Euler integration with a time step $\Delta t = 0.002\ ms$ was used to integrate the system of differential equations governing the cellular electrical behavior. The Rush and Larsen integration scheme (Rush and Larsen, 1978) was used to integrate the Hodgkin-Huxley type equations for the gating variables of the various time-dependent currents (m, h, and j for I_{Na}; x_{to_f}, x_{to_s}, y_{to_f} and y_{to_s} for I_{to}; x_{kr} for I_{Kr}; x_{ks} for I_{Ks} and d, f and f_2 for I_{CaL}).

In the hyperkalemia study, a $4\ cm$ long multicellular fiber was used. For the simulations, the operator splitting techique was implemented for solving the reaction-diffusion equation that describes the conduction along a cable. The same integration scheme used in isolated cells was used in this case. Implicit Euler with a time step $\Delta t = 0.002\, ms$ and a mesh size $\Delta x = 0.1\, mm$ was used to integrate the parabolic equation. To obtain a maximum planar CV of $74\ cm/s$ (Taggart et al., 2000), a cellular conduction of $0.0013\ cm^2/ms$ was required. Five positions within the fiber were selected for further analysis in each simulation. These positions were located at 1.5, 1.75, 2, 2.25 and 2.5 from the stimulation end of the cable. The APD and the CV were computed as their mean values over these positions.

4.2 Results for Control Conditions

4.2.1 Biomarkers of arrhythmic risk

Table 4.1 shows the computed biomarkers for the modified CRLP model. Results are compared against those obtained with previous models (TP06 and GPB) and against a variety of physiological data described in (Beuckelmann et al., 1992; Drouin et al., 1995; Franz et al., 1988; Li et al., 1998, 1999; Nash et al., 2006; Pieske et al., 1999, 2002; Schmidt et al., 1998).

These results indicate that the GPB model performs better than the TP06 model with respect to the following biomarkers: triangulation, systolic and diastolic $[Ca^{2+}]_i$ at 0.5 Hz and rate dependence of steady-state $[Na^{+}]_i$ and $[Ca^{2+}]_i$. However, according to other analyzed biomarkers, the GPB model renders worse results than the TP06 model. Specifically, in (Franz et al., 1988) two phases of APD rate adaptation were

Biomarker	TP06	GPB	CRLP	Physiolo.
APD_{90}	301.2	285.0	305.6	271-366
Triangulation	28.4	51.5	78	44-112
Sys $[Ca^{2+}]_i$ 1 Hz	0.886	0.383	0.602	1.59-2.01
Sys $[Ca^{2+}]_i$ 0.5 Hz	0.199	0.345	0.523	0.71-1.68
Dia $[Ca^{2+}]_i$ 1 HZ	0.104	0.089	0.097	0.20-0.33
Dia $[Ca^{2+}]_i$ 0.5 Hz	0.068	0.085	0.091	0.14-0.32
$S_{max_{S1S2}}$	1.3	0.2	1.0	0.79-4.25
$S_{max_{DYN}}$	1.0	1.1	0.9	---
τ_{fast}	13.3	---	10.2	---
τ_{slow}	124.8	56.3	105.6	70-110
Max. sys. $[Ca^{2+}]_i$	1157	178	147	130-170
Max. sys. $[Na^{+}]_i$	217	132	134	145

Table 4.1. Biomarkers of arrhythmic risk for the TP06, GPB and CRLP human models. Green color indicates within physiological range. Blue color indicates out of physiological range but better than previous models. Red color indicates out of physiological range.

reported: a first phase with a short time constant and a second phase with a longer time constant. The APD rate response in the GPB model does not present this first phase. Also, the S1S2 restitution curves of the TP06 model (Figure 4.1.c) are in better agreement with experimental data.

For the CRLP model, most of the twelve analyzed biomarkers are within physiological range or otherwise closer to the physiological range as compared to GPB and TP06 models, except for systolic and diastolic $[Ca^{2+}]_i$ levels at 1 Hz, where TP06 outperforms CRLP.

4.2.2 Blocking Currents

We have also studied the behavior of the model under total and partial block of potassium currents, comparing the results against those reported in (Jost et al., 2008) from experiments in human ventricle:

- I_{Ks}: To simulate the effect of $1\ \mu M$ of HMR-1556, I_{Ks} was completely blocked.
- I_{Kr}: To simulate the effect of $50\ nM$ of dofetilide, I_{Kr} was completely blocked.
- I_{K1}: To simulate the effect of $10\ \mu M$ of $BaCl_2$, I_{K1} was reduced by 50%.

Table 4.2 summarizes the effect of current block on the different models. Results are given as percentage of variation of the APD value in control conditions. In those cases where more than one current is blocked, the variation refers to the APD obtained when the first current is blocked. Experimental values have been taken from (Jost et al., 2008).

In Figure 4.2 the efects of the different blocks for the original and the modified models are represented.

4.3 Results for Hyperkalemic Conditions

For the simulation of hyperkalemia a 1-dimensional fiber was used, as described in section 4.1. Hyperkalemic conditions were simulated by increasing the extracellular K^+ concentration from 4.0 mM to 15 mM (depending on the degree of simulated hyperkalemia).

The stimulation protocol consisted of a train of ten basic stimulations (S1) with a cyclic length of 1,000 ms, followed by an extrasystole stimulus (S2) delivered at different times taken in 0.1 millisecond steps in order to determine ERP. CV and APD were measured after the last S1 stimulus.

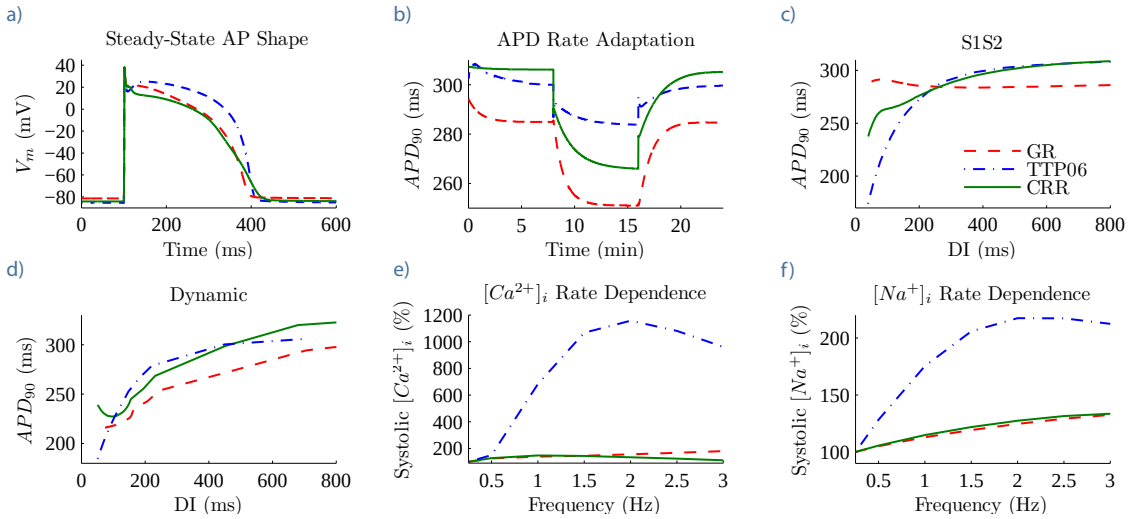

Figure 4.1. Biomarkers of arrhythmic risk from TP06, GPB and CRLP models: a) AP for CL = 1000 ms; b) APD rate adaptation to abrupt changes in CL (From 1000 ms to 600 ms); c) S1S2 restitution protocol curve; d) Dynamic restitution protocol curve; e) rate dependence of steady-state $[Na^{+}]_i$; f) Rate dependence of steady-state $[Ca^{2+}]_i$

Current		Ref.	TT	GPB	CRLP	Exper.
I_{Kr}	0%	Control	74.9	0.7	0.6	< 2.8
I_{Kr}	0%	Control	15.9	18.6	14.1	44±4
I_{Ks} I_{Kr}	0% 0%	I_{Kr} B.	---	1.4	0.8	9
I_{K1}	50%	Control	3.6	11.5	14.6	4.8±1.5
I_{Kr} I_{K1}	0% 50%	I_{Kr} B.	8.9	15.6	21.1	33

Table 4.2. Percentages of variation in the APD caused by blocking different currents. Green color indicates within physiological range. Blue color indicates out of physiological range but better than previous models. Red color indicate out of physiological range.

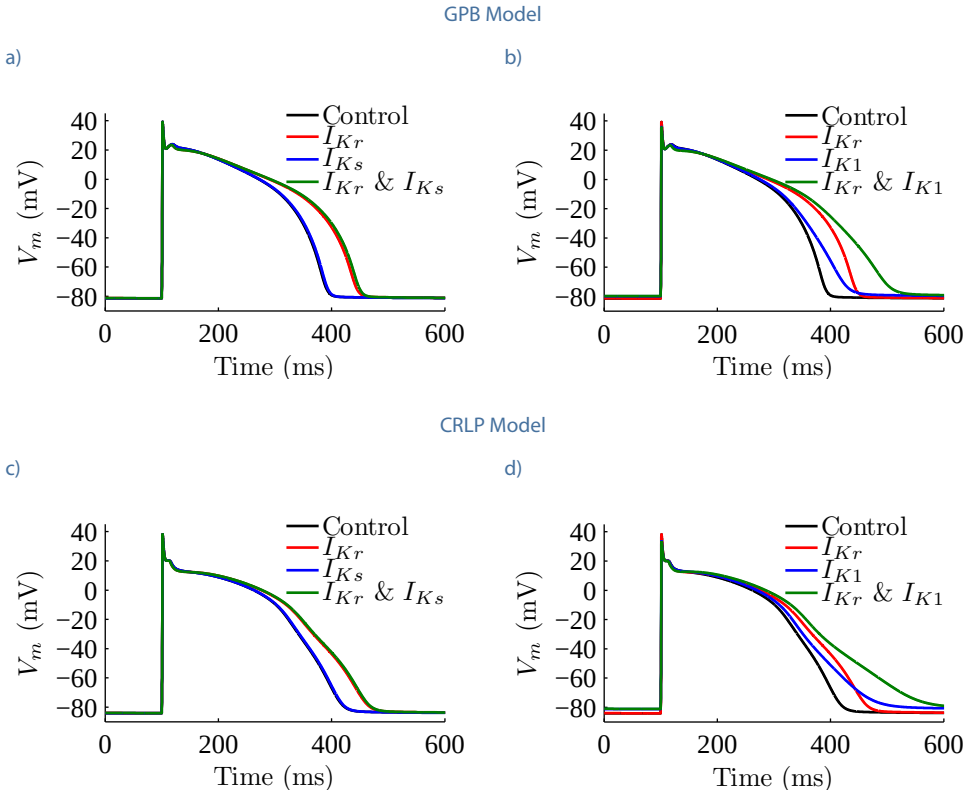

Figure 4.2. Blocking currents for the GPB and CRLP models: a) Effect of completely blocking I_{Kr} and I_{Ks} currents in the GPB model, b) Effect of completely blocking I_{Kr} and partialy blocking I_{K1} in the GPB model, b) Effect of completely blocking I_{Kr} and I_{Ks} currents in the CRLP model, b) Effect of completely blocking I_{Kr} and partially blocking I_{K1} in the CRLP model.

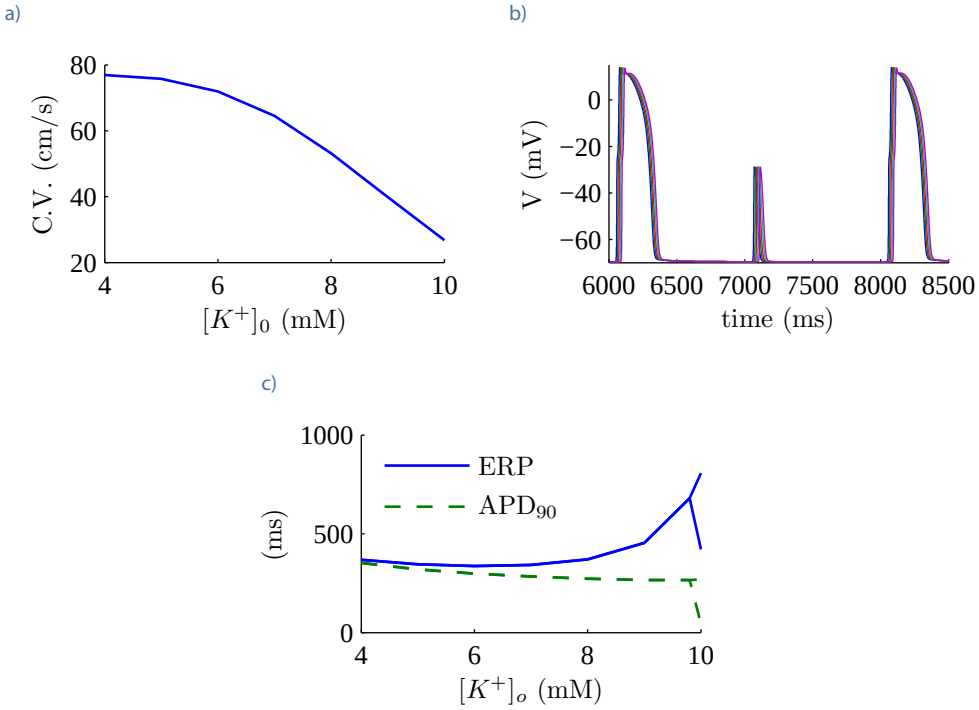

Figure 4.3. Behavior of the model under hyperkalemic conditions in 1-D fiber: a) conduction velocity versus $[K^+]_o$; b) example of alternans for $[K^+]_o = 10.0\,mM$, each color represents a different position in the fiber; c) dependence of ERP and APD with the $[K^+]_o$.

The basic stimuli consisted of rectangular pulses of 3 ms duration and 1.5 times the diastolic threshold. This threshold was determined as follows. For a given $[K^+]_o$ value, the model was first stabilized until when the product of the gates $h \cdot j$ reached 99% of the steady-state value $h_{ss} \cdot j_{ss}$. Once the model had reached steady-state conditions, an stimulation current was applied at the left end of the cable. Diastolic threshold was defined as the minimum stimulation current required in order for an action potential to propagate along the cable.

4.3.1 Conduction Velocity

Figure 4.3.a shows CV obtained for different values of $[K^+]_o$. In our proposed CRLP model, as in TP06, there is no supernormal conduction (Shaw and Rudy, 1997) (Kagiyama et al., 1982). Above 10.4 mM there is no conduction and over 9.8 mM alternans appeared (Figure 4.3.b).

4.3.2 Action Potential Duration and Effective Refractory Period

Figure 4.3.c shows APD and ERP measurements for different values of $[K^+]_o$. APD decreases when the extracellular K^+ concentration increases. For high $[K^+]$ values, the APD curve is divided into two branches, which is explained by the ocurrence of alternans at those high concentrations.

The ERP has three phases. In the first one, ERP decreases with APD. After this, ERP begins to increase (the excitability of the cells decreases due to the increase in $[K^+]_o$). Finally, the last phase is caused by the ocurrence of alternans. Depending on whether the beat that is measured is an odd or an even beat, ERP takes one or another value.

Chapter 5

Discussion and conclusions

In this study a new human ventricular cell model has been developed, which is suitable for investigation of cardiac arrhythmias. Taking the recently proposed GPB model as a starting point, several modifications have been introduced by accounting for recent experimental measurements of potassium currents, and by reformulating the L-type calcium current so as to introduce fast and slow voltage-dependent inactivation. All the modifications have been made with the aim of maintaining the advantages that the GPB model presents over previous models, such as the TP06 model, while improving the performance on other electrophysiological aspects. The novelty of this study is that the development of our proposed CRLP model is not only based on new data from experiments of ionic currents. More importantly, the development is also based on the results of several arrhythmic risk biomarkers reported in the literature.

For the proposed CRLP model, the introduction of fast and slow I_{CaL} inactivation has led to a more physiological rate adaptation response as compared to the original GPB model. The other modifications have rendered most biomarkers to be within the physiological range or otherwise closer to the physiological range as compared to the GPB and TP06 models, except for systolic and diastolic $[Ca^{2+}]_i$ levels at 1 Hz where TP06 outperforms CRLP. These modifications, however, have altered the behavior of the model against current blocks minimally, thus providing results in very good agreement with available experimental data.

The results of the analysis conducted in this study points out the importance that calcium dynamics have over different biomarkers. This suggests the need for continuing with the development of more reliable calcium dynamic models that allow improving the performance of whole cell AP models.

The hyperkalemia simulations showed that APD progressively decreased with the level of hyperkalemia, while ERP increased after a threshold in the extracellular $[K^+]$ was reached ($[K^+]_o = 6\,mM$). Conduction velocity decreased with hyperkalemia and the conduction was blocked above $[K^+]_o = 10.4\,mM$. Additionally, alternans appeared in the APD above $[K^+]_o = 9.8\,mM$. These results suggest that the longer ERP values and the conduction blocking above $[K^+]_o = 10.4\,mM$ found in the central zone of acutely ischemic tissue as compared to the normal zone could create areas of block that could set the stage for reentrant arrhythmias.

Future develpments of the model will include a complete ischemic model with ATP sensitive potassium current (I_{KATP}) and simulations of acidosis. The simulations with the model will be made, not only in a 1-D fiber but in 2-D tissue and in a realistic human ventricular geometry.

Bibliography

Bibliography

J. Benitah, P. Bailly, M. D'Agrosa, J. Da Ponte, C. Delgado, and P. Lorente. Slow inward current in single cells isolated from adult human ventricles. *Pflügers Arch*, 421:176--187, 1992.

M. O. Bernabeu, R. Bordas, P. Pathmanathan, J. Pitt-Francis, J. Cooper, A. Garny, D. J. Gavaghan, B. Rodríguez, J. A. Southern, and J. P. Whiteley. Chaste: Incorporating a novel multiscale spatial and temporal algorithm into a large scale open source library. *Phil Trans Roy Soc (A)*, 367(1895):1907--1930, 2009.

D. M. Bers and S. Despa. Cardiac myocytes ca2+ and na+ regulation in normal and failing hearts. *J Pharm Sci*, 100:315--322, 2006.

D. J. Beuckelmann, M. Näbauer, and E. Erdmann. Characteristics of calcium-current in isolated human ventricular myocytes from patients with terminal heart failure. *J Clin Invest*, 23:929 -- 937, 1991. ISSN 0022-2828.

D. J. Beuckelmann, M. Nabauer, and E. Erdmann. Intracellular calcium handling in isolated ventricular myocytes from patients with terminal heart failure. *Am Heart J*, 85:1046--1055, 1992.

E. Carmeliet. Cardiac ionic currents and acute ischemia: from channels to arrhythmias. *Physiol Rev*, 79:917--1017, 1999.

M. Courtemanche, R. J. Ramirez, and S. Nattel. Ionic mechanisms underlying human atrial action potential properties: insights from a mathematical model. *Am J Physiol Heart Circ Physiol*, 275:301--321, 1998.

I. Dodama, A. Wilde, M. J. Janse, D. Durrer, and K. Yamada. Combined effects of hypoxia, hyperkalemia and acidosis on membrane action potential and excitability of guinea-pig ventricular muscle. *Academic Press Inc.*, 1984.

E. Drouin, F. Charpentier, C. Gauthier, K. Laurent, and H. L. Marec. Electrophysiologic characteristics of cells spanning the left ventricular wall of human heart: Evidence for presence of m cells. *J Am Coll Cardiol*, 26: 185 -- 192, 1995.

M. Fink, D. Noble, L. Virag, A. Varro, and W. R. Giles. Contributions of herg k+ current to repolarization of the human ventricular action potential. *Progress in Biophysics and Molecular Biology*, 96:357 -- 376, 2008. ISSN 0079-6107.

M. R. Franz, C. D. Swerdlow, L. B. Liem, and J. Schaefer. Cycle length dependence of human action potential duration in vivo. *Am Clin Inves*, 82:972--979, 1988.

R. J. Gilmour and D. Zipes. Different electrophysiological responses of canine endocardium and epicardium to combined hyperkalemia, hypoxia, and acidosis. *Circulation Research*, 46:814--825, 1980.

E. Grandi, F. S. Pasqualini, and D. M. Bers. A novel computational model of the human ventricular action potential and ca transient. *J Mol Cell Cardiol*, 48:112 -- 121, 2010.

L. Hondeghem, L. Carlsson, and G. Duker. Instability and triangulation of the action potential preict serious proarrhythmia, but action potential duration prolongation is antiarrhythmic. *Circ*, 103:2004--2013, 2001.

V. Iyer, R. Mazhari, and R. Winslow. Computational model of the human leftventricular epicardial myocyte. *Biophys J*, 87(3):1507--1525, 2004.

N. Jost, A. Varro, V. Szuts, P. P. Kovacs, G. Seprényi, P. Biliczki, C. Lengyel, J. Prorok, M. Bitay, B. Ördög, J. Szabad, Z. Varga-Orvos, L. Puskas, D. Cotella, J. G. Papp, L. Virag, and S. Nattel. Molecular basis of repolarization reserve differences between dogs and man. *Circ*, 118 Suppl-2:S342 (abstract), 2008.

Y. Kagiyama, J. Hill, and L. Gettes. Interaction of acidosis and increased extracellular potassium on action potential epicardium to combined hyperkalemia, hypoxia, and acidosis. *Circ Res*, 51:614--623, 1982.

H. Kishida, B. Surawicz, and L. Fu. Effects of k+ and k+-induced polarization on (dv/dt)max, threshold potential, and membrane input resistance in guinea pig and cat ventricular myocardium. *Circ Res*, 44:800--814, 1979.

A. Levi, G. Dalton, J. Hancox, J. Mitcheson, J. Issberner, J. Bates, S. Evans, F. Howarth, I. Hobai, and J. Jones. Role of intracellular sodium overload in the genesis of cardiac arrhythmias. *J Cardiovasc Electrophysiol*, 8: 700--721, 1997.

G.-R. Li, J. Feng, L. Yue, and M. Carrier. Transmural heterogeneity of action potentials and ito1 in myocytes isolated from the human right ventricle. *Am J Physiol Heart Circ Physiol*, 275:H369--377, 1998.

G.-R. Li, B. Yang, J. Feng, R. F. Bosch, M. Carrier, and S. Nattel. Transmembrane ica contributes to rate-dependent changes of action potentials in human ventricular myocytes. *Am J Physiol Heart Circ Physiol*, 276:H98--106, 1999.

C. Luo and Y. Rudy. A model of the ventricular cardiac action potential: Depolarization, repolarization and their interaction. *Circulation Research*, 68:1501--1526, 1991.

C. Luo and Y. Rudy. A dynamic model of the cardiac ventricular action potential: I. simulations of ionic currents and concentration changes. *Circulation Research*, 74:1071--1096, 1994.

J. Magyar, N. Iost, Á. Körtvély, T. Bányász, L. Virág, P. Szigligeti, A. Varró, M. Opincariu, J. Szécsi, J. G. Papp, and P. P. Nánási. Effects of endothelin-1 on calcium and potassium currents in undiseased human ventricular myocytes. *Pflügers Arch*, 441:144--149, 2000.

M. M. Maleckar, J. L. Greenstein, W. R. Giles, and N. A. Trayanova. K+ current changes account for the rate dependence of the action potential in the human atrial myocyte. *Am J Physiol Heart Circ Physiol*, 297: 1298--1410, 2009.

T. Mewes and U. Ravens. L-type calcium currents of human myocytes from ventricle of non-failing hearts and atrium. *J Mol Cell Cardiol*, 26:1307--1320, 1994.

E. Murphy and D. Eisner. Regulation of intracellular and mitochondiral sodium in health and disease. *Circ Res*, 104:292--303, 2009.

M. Nash, C. Gradley, P. Sutto, R. Clayton, P. Kallis, M. Hayward, D. Paterson, and P. Taggart. Whole heart action potential duration restitution properties in cardiac patients: a combined clinical and modeling study. *Exp Physiol*, 91:339--354, 2006.

D. Noble. Cardiac action and pacemaker potentials based on the hodgkin-huxley equations. *Nature*, 188: 495--497, 1960.

D. Noble, A. Varghese, P. Kohl, and N. P. Improved guinea-pig ventricular cell model incorporating a diadic space, ikr and iks, and length- and tension-dependent processes. *Can J Cardiol*, 14(1):123--134, 1998.

J. Nolasco and R. Dahlen. A graphic method for the study of alternation in cardiac action potentials. *J Appl Physiol*, 25:191--196, 1968.

B. Pelzmann, P. Schaffer, E. Bernhart, P. Lang, H. Machler, B. Rigler, and B. Koidl. L-type calcium current in human ventricular myocytes at a physiological temperature from children with tetralogy of fallot. *Cardiovasc Res*, 38:424--432, 1998.

B. Pieske, L. Maier, D. Bers, and G. Hasenfuss. Ca2+ handling and sarcoplasmic reticulum ca2+ content in isolated failing and nonfailing human myocardium. *Circ Res*, 85:38--46, 1999.

B. Pieske, L. Maier, V. r. Piacentino, J. Weisser, G. Hasenfuss, and S. Houser. Rate dependence of $[na^+]_i$ and contractility in nonfailing and failing human myocardium. *Circ*, 106:447--453, 2002.

R. Plonsey and J. Malmivuo. *Bioelectromagnetism - Principles and Applications of Bioelectric and Biomagnetic Fields*. Oxford University Press, 1995.

E. Pueyo, P. Smetana, P. Caminal, A. de Luna, M. Malik, and P. Laguna. Characterization of qt interval adaptation to rr interval changes and its use as a risk-stratifier of arrhythmic mortality in amiodarone-treated survivors of acute myocardial infarction. *IEEE Trans Biomed Eng*, 51:1511--1520, 2004.

E. Pueyo, Z. Husti, T. Hornyik, I. Baczkó, P. Laguna, A. Varró, and B. Rodríguez. Mechanisms of ventricular rate adaptation as a predictor of arrhythmic risk. *Am J Physiol Heart Circ Physiol*, 298:H1577--H1587, 2010.

L. Romero, E. Pueyo, M. Fink, and B. Rodríguez. Impact of ionic current variability on human ventricular cellular electrophysiology. *Am J Physiol Heart Circ Physiol*, 297:H1436--1445, 2009.

S. Rush and H. Larsen. A practical algorithm for solving dynamic membrane equations. *Biomedical Engineering, IEEE Transactions on*, BME-25(4):389 --392, 1978.

U. Schmidt, R. Hajjar, P. Helm, C. Kim, A. Doye, and J. Gwathmey. Contribution of abnormal sarcoplasmic reticulum atpase activity to systolic and diastolic dysfunction in human heart failure. *J Mol Cell Cardiol*, 30: 1929--1937, 1998.

J. Senges, J. Brachmann, D. Pelzer, T. Mizutani, and W. Kubler. Effects of some components of ischemia on electrical activity and reentry in the canine ventricular conducting system. *Circ Res*, 44:864--872, 1979.

R. M. Shaw and Y. Rudy. Electrophysiologic effects of acute myocardial ischemia: A mechanistic investigation of action potential conduction and conduction failure. *Circ R*, 80:124--138, 1997.

H. Sun, N. Leblanc, and S. Nattel. Mechanisms of inactivation of l-type calcium channels in human atrial myocytes. *Am J Physiol Heart Circ Physiol*, 33:H1625--H1635, 1997.

P. Taggart, P. Sutton, T. Opthof, R. Coronel, R. Trimlett, and W. Pugsley. Inhomogeneous transmural conduction during early ischemia in patients with coronary artery disease. *J Mol Cell Cardiol*, 32:621--639, 2000.

K. ten Tusscher. *Spiral wave dynamics and ventricular arrhythmias*. PhD thesis, Utrecht University, 2004.

K. ten Tusscher and A. Panfilov. Alternans and spiral breakup in a human ventricular tissue model. *Am J Physiol Heart Circ Physiol*, 291:H1088--H1100, 2006.

K. H. W. J. ten Tusscher, D. Noble, P. J. Noble, and A. V. Panfilov. A model for human ventricular tissue. *Am J Physiol Heart Circ Physiol*, 286(4):H1573--1589, 2004.

R. Tian and J. Ingwall. Energetic basis for reduced contractile reserve in isolated rat hearts. *Am J Physiol Heart Circ Physiol*, 270:H1207--H1216, 1196.

A. Vleugels, J. Vereecke, and E. Carmeliet. Ionic currents during hypoxia in voltage-clamped cat ventricular muscle. *Circ Res*, 47:501--508, 1980.

P. Volders, M. Vos, B. Szabo, K. Sipido, S. de Groot, A. Gorgels, H. Wellens, and R. Lazzara. Progress in the understanding of cardiac early afterdepolarizations and torsades de pointes: time to revise current concepts. *Cardiovasc Res*, 46:376--392, 2000.

J. Weiss, A. Karma, U. Shiferaw, P. Chen, A. Garfinkel, and Z. Qu. From pulses to pulseless: the saga of cardiac alternans. *Circ Res*, 98:1244--1253, 2006.

Clinical Practice

Clinical Practice

The clinical practice of the study was conducted at *Hospital Clínico de Valencia*. It was divided into two parts. The first part was carried out in collaboration with the group directed by Dr. Ricardo Ruiz Granell in the Cardiostimulation Unit. The second part was conducted in the research group led by Dr. Francisco Javier Chorro about the investigation of different pathologies using rabbit hearts.

In the first part of the clinical practice with the group of Dr. Ricardo Ruiz, several interventions were witnessed. Some cardioversions were performed by team doctors, where different types of arrhythmias were terminated by delivering a synchronized shock. Likewise, different checks and follow-ups of pacemakers and defibrillators were witnessed.

Also, an intervention in a patient with history of chronic ischemic arrhythmia took place during the days of the internship. In that intervention an ablation of the part of the heart causing reentrant circuits was performed. For this, first of all, a 3D map of the inside of the heart and its electrical activity was measured. An arrhythmia was induced with an extra-stimulus test to check its focus and, finally, all the identified zone was burned in order to prevent the spread of late fronts.

During the days of the clinical practice, different conversations on the applicability of the investigation with computational models took place between the student and the doctors. In this conversations the doctors proposed the application of our model to the investigation of arrhythmias caused by genetic diseases like Brugada syndrome, where some channels present a pathological behavior and are common in the clinical routine. Other pathologies like arrhythmias caused by acute ichemia were very rare to find in the clinic because usually the patient does not survive to reach the hospital and in case it happens, the procedure is clear, to deliver an electroshock.

During the second part of the clinical practice with the group led by Dr. Francisco Javier Chorro, some experiments in rabbit hearts were witnessed. This group is currently working in the study of the differences between the heart response in rabbits trained and not trained. Likewise, they are working on comparing the electrophysiology of the heart in control conditions and when it is subjected to stretch. In this studies they are using an increasing stimulation frequency to generate arrhythmias and the extra-stimulus test to study CV and ERP. With a sensor they perform an electrical mapping in the surface of the heart and they process the measures to create activation maps. For all these experiments they use a Langendorff system that allows them to mantain the heart alive after having been extracted from the body. With this clinical practice it was posible to see a real application of the same procedures used in the simulations conducted in this study.

Appendices

Appendix A

Human Ventricular Cell Model

A.1 Model Parameters

A.1.1 Physical Constants

Name	Value	Units
R	8314	$J/(mol \cdot K)$
$Frdy$	96485	C/mol
T	310	K
$FoRT$	$Frdy/(R \cdot T)$	mV^{-1}
C_{mem}	$1.381 \cdot 10^{-10}$	F

A.1.2 Enviromental Parameters

Name	Value	Units
$Length_{cell}$	$100 \cdot 10^{-5}$	dm
$Radius_{cell}$	$10.25 \cdot 10^{-5}$	dm
V_{cell}	$\pi \cdot Radius_{cell}^2 \cdot Length_{cell}$	L
V_{myo}	$0.65 \cdot V_{cell}$	L
V_{sr}	$0.035 \cdot V_{cell}$	L
V_{sl}	$0.02 \cdot V_{cell}$	L
V_{junc}	$5.39 \cdot 10^{-4} \cdot V_{cell}$	L
$J_{Ca_{junc,sl}}$	$8.2413 \cdot 10^{-13}$	L/ms
$J_{Ca_{sl,myo}}$	$3.7243 \cdot 10^{-12}$	L/ms
$J_{Na_{junc,sl}}$	$1.8313 \cdot 10^{-14}$	L/ms
$J_{Na_{sl,myo}}$	$1.6386 \cdot 10^{-12}$	L/ms

A.1.3 Fractional Currents

Name	Value	Units
F_{junc}	0.11	$[-]$
F_{sl}	$1 - F_{junc}$	$[-]$
$F_{junc_{Ca_L}}$	0.9	$[-]$
$F_{sl_{Ca_L}}$	$1 - F_{junc_{Ca_L}}$	$[-]$

A.1.4 Ion Concentrations

Name	Value	Units
K_i	138	mM
K_o	5.4	mM
Cl_i	15	mM
Cl_o	150	mM
Ca_o	1.8	mM
Mg_i	1	mM
Na_o	140	mM

A.1.5 Sodium Transport

Name	Value	Units
G_{Na}	18.86	$mS/\mu F$
G_{NaB}	$0.597 \cdot 10^{-3}$	$mS/\mu F$
$\bar{I}_{NaK}$	0.99	pA/pF
Km_{Ko}	1.5	mM
Km_{Naip}	11	mM

A.1.6 Potassium Currents

Name	Value	Units
p_{NaK}	$1.833 \cdot 10^{-2}$	$[-]$
G_{K1}	$5.7153 \cdot 10^{-1}$	$mS/\mu F$
G_{Kp}	$2 \cdot 10^{-3}$	$mS/\mu F$
G_{Kr}	$3.5 \cdot 10^{-2}$	$mS/\mu F$
$G_{Ks_{junc}}$	$3.5 \cdot 10^{-3}$	$mS/\mu F$
$G_{Ks_{sl}}$	$3.5 \cdot 10^{-3}$	$mS/\mu F$
$G_{to_f,EPI}$	$1.144 \cdot 10^{-1}$	$mS/\mu F$
$G_{to_s,EPI}$	$1.56 \cdot 10^{-2}$	$mS/\mu F$
$G_{to_f,ENDO}$	$1.404 \cdot 10^{-3}$	$mS/\mu F$
$G_{to_s,ENDO}$	$3.7596 \cdot 10^{-2}$	$mS/\mu F$

A.1.7 Chlorine currents

Name	Value	Units
G_{ClCa}	0.054813	$mS/\mu F$
G_{ClB}	$9 \cdot 10^{-3}$	$mS/\mu F$
Kd_{ClCa}	$100 \cdot 10^{-3}$	mM

A.1.8 Calcium Transport

Name	Value	Units
p_{Ca}	$1.9887 \cdot 10^{-4}$	$L/(F \cdot ms)$
p_{K}	$5.4675 \cdot 10^{-8}$	$L/(F \cdot ms)$
p_{Na}	$3.0375 \cdot 10^{-9}$	$L/(F \cdot ms)$
$\bar{I}_{NCX}$	4.5	pA/pF
Km_{Ca_i}	$3.59 \cdot 10^{-3}$	mM
Km_{Ca_o}	1.3	mM
Km_{Na_i}	12.29	mM
Km_{Na_o}	87.5	mM
k_{sat}	0.32	$[-]$
nu	0.27	$[-]$
Kd_{act}	$0.15 \cdot 10^{-3}$	mM
$\bar{I}_{PMCA}$	0.0673	pA/pF
Km_{pCa}	$0.5 \cdot 10^{-3}$	mM
G_{CaB}	$5.513 \cdot 10^{-4}$	$mS/\mu F$

A.1.9 SR Calcium Fluxes

Name	Value	Units
$V_{max_{SR_{CaP}}}$	$5.3114 \cdot 10^{-3}$	mM/ms
$ec50_{SR}$	0.45	mM
$hill_{SR_{CaP}}$	1.787	$[-]$
ki_{Ca}	0.5	$mM^{-1} \cdot mS^{-1}$
ki_{m}	0.005	mS^{-1}
ko_{Ca}	10	$mM^{-2} \cdot ms^{-1}$
ko_{m}	0.06	mS^{-1}
ks	25	mS^{-1}
Km_{f}	$0.246 \cdot 10^{-3}$	mM
Km_{r}	1.7	mM
Max_{SR}	15	$[-]$
Min_{SR}	1	$[-]$

A.1.10 Buffering

Name	Value	Units
$B_{max_{CaM}}$	$24 \cdot 10^{-3}$	mM
$B_{max_{SR}}$	$17.1 \cdot 10^{-3}$	mM
$B_{max_{TnC_{high}}}$	$140 \cdot 10^{-3}$	mM
$B_{max_{TnC_{low}}}$	$70 \cdot 10^{-3}$	mM
$B_{max_{myosin}}$	$140 \cdot 10^{-3}$	mM
$B_{max_{Na_j}}$	7.561	mM
$B_{max_{Na_{sl}}}$	1.65	mM
$B_{max_{SL_{low_{sl}}}}$	$37.4 \cdot 10^{-3} \cdot V_{myo}/V_{sl}$	mM
$B_{max_{SL_{low_j}}}$	$4.6 \cdot 10^{-4} \cdot V_{myo}/V_{junc}$	mM
$B_{max_{SL_{high_{sl}}}}$	$13.4 \cdot 10^{-3} \cdot V_{myo}/V_{sl}$	mM
$B_{max_{SL_{high_j}}}$	$1.65 \cdot 10^{-4} \cdot V_{myo}/V_{junc}$	mM
$B_{max_{csqn}}$	$140 \cdot 10^{-3} \cdot V_{myo}/V_{sr}$	mM
$k_{off_{csqn}}$	65	mS^{-1}
$k_{off_{CaM}}$	$238 \cdot 10^{-3}$	mS^{-1}
$k_{off_{SR}}$	$60 \cdot 10^{-3}$	mS^{-1}
$k_{off_{TnC_{h_{Ca}}}}$	$0.032 \cdot 10^{-3}$	mS^{-1}
$k_{off_{TnC_{h_{Mg}}}}$	$3.33 \cdot 10^{-3}$	mS^{-1}
$k_{off_{TnC_l}}$	$19.6 \cdot 10^{-3}$	mS^{-1}
$k_{off_{myo_{Ca}}}$	$0.46 \cdot 10^{-3}$	mS^{-1}
$k_{off_{myo_{Mg}}}$	$0.057 \cdot 10^{-3}$	mS^{-1}
$k_{off_{sl_h}}$	$30 \cdot 10^{-3}$	mS^{-1}
$k_{off_{sl_l}}$	1.3	mS^{-1}
$k_{off_{Na}}$	$1 \cdot 10^{-3}$	mS^{-1}
$k_{on_{csqn}}$	100	$mM^{-1} \cdot mS^{-1}$
$k_{on_{CaM}}$	34	$mM^{-1} \cdot mS^{-1}$
$k_{on_{SR}}$	100	$mM^{-1} \cdot mS^{-1}$
$k_{on_{TnC_{h_{Ca}}}}$	2.37	$mM^{-1} \cdot mS^{-1}$
$k_{on_{TnC_{h_{Mg}}}}$	$3 \cdot 10^{-3}$	$mM^{-1} \cdot mS^{-1}$
$k_{on_{TnC_l}}$	32.7	$mM^{-1} \cdot mS^{-1}$
$k_{on_{myo_{Ca}}}$	13.8	$mM^{-1} \cdot mS^{-1}$
$k_{on_{myo_{Mg}}}$	0.0157	$mM^{-1} \cdot mS^{-1}$
$k_{on_{sl_h}}$	100	$mM^{-1} \cdot mS^{-1}$
$k_{on_{sl_l}}$	100	$mM^{-1} \cdot mS^{-1}$
$k_{on_{Na}}$	$0.1 \cdot 10^{-3}$	$mM^{-1} \cdot mS^{-1}$

A.2 Model Equations

A.2.1 Nerst Potentials

$$
\begin{aligned}
E_{Na_{junc}} &= \frac{1}{FoRT} \cdot \ln \frac{Na_o}{Na_j} \\
E_{Na_{sl}} &= \frac{1}{FoRT} \cdot \ln \frac{Na_o}{Na_{sl}} \\
E_{Ks} &= \frac{1}{FoRT} \cdot \ln \frac{K_o + p_{NaK} \cdot Na_o}{K_i + p_{NaK} \cdot Na_i} \\
E_K &= \frac{1}{FoRT} \cdot \ln \frac{K_o}{K_i} \\
E_{Ca_{junc}} &= \frac{1}{2 \cdot FoRT} \cdot \ln \frac{Ca_o}{Ca_j} \\
E_{Ca_{sl}} &= \frac{1}{2 \cdot FoRT} \cdot \ln \frac{Ca_o}{Ca_{sl}} \\
E_{Cl} &= \frac{1}{FoRT} \cdot \ln \frac{Cl_i}{Cl_o}
\end{aligned}
$$

A.2.2 I_{Na}:Fast Sodium Current

$$
\begin{aligned}
m_{ss} &= \frac{1}{\left(1 + e^{\frac{-(56.86 + V_m)}{9.03}}\right)^2} \\
\tau_m &= 0.1292 \cdot e^{-\left(\frac{V_m + 45.79}{15.54}\right)^2} + 0.06487 \cdot e^{-\left(\frac{V_m - 4.823}{51.12}\right)^2} \\
\frac{\mathrm{d}m}{\mathrm{d}t} &= \frac{m_{ss} - m}{\tau_m}
\end{aligned}
$$

$$
\begin{aligned}
a_h &= \begin{cases} 0 & \text{if } V_m \geq -40 \\ 0.057 \cdot e^{\frac{-(V_m + 80)}{6.8}} & \text{otherwise} \end{cases} \\
b_h &= \begin{cases} \frac{5.9231}{1 + e^{\frac{-(V_m + 10.66)}{11.1}}} & \text{if } V_m \geq -40 \\ 2.7 \cdot e^{0.079 \cdot V_m} + 3.1 \cdot 10^5 \cdot e^{0.3485 \cdot V_m} & \text{otherwise} \end{cases} \\
\tau_h &= \frac{1}{a_h + b_h} \\
h_{ss} &= \frac{1}{\left(1 + e^{\frac{V_m + 71.55}{7.43}}\right)^2} \\
\frac{\mathrm{d}h}{\mathrm{d}t} &= \frac{h_{ss} - h}{\tau_h}
\end{aligned}
$$

$$
\begin{aligned}
a_j &= \begin{cases} 0 & \text{if } V_m \geq -40 \\ \frac{\left(-2.5428\cdot 10^4\cdot e^{0.2444\cdot V_m} - 6.948\cdot 10^{-6}\cdot e^{-0.04391\cdot V_m}\right)\cdot (V_m+37.78)}{1+e^{0.311\cdot (V_m+79.23)}} & \text{otherwise} \end{cases} \\
b_j &= \begin{cases} \frac{0.6\cdot e^{0.057\cdot V_m}}{1+e^{-0.1\cdot (V_m+32)}} & \text{if } V_m \geq -40 \\ \frac{0.02424\cdot e^{-0.01052\cdot V_m}}{1+e^{-0.1378\cdot (V_m+40.14)}} & \text{otherwise} \end{cases} \\
\tau_j &= \frac{1}{a_j + b_j} \\
j_{ss} &= \frac{1}{\left(1+e^{\frac{V_m+71.55}{7.43}}\right)^2} \\
\frac{\mathrm{d}j}{\mathrm{d}t} &= \frac{j_{ss}-j}{\tau_j}
\end{aligned}
$$

$$
\begin{aligned}
I_{Na_{junc}} &= F_{junc}\cdot G_{Na}\cdot m^3\cdot h\cdot j\cdot \left(V_m - E_{Na_{junc}}\right) \\
I_{Na_{sl}} &= F_{sl}\cdot G_{Na}\cdot m^3\cdot h\cdot j\cdot \left(V_m - E_{Na_{sl}}\right) \\
I_{Na} &= I_{Na_{junc}} + I_{Na_{sl}}
\end{aligned}
$$

A.2.3 I_{NaBk}: Background Sodium Current

$$
\begin{aligned}
I_{NaBk_{junc}} &= F_{junc}\cdot G_{NaB}\cdot \left(V_m - E_{Na_{junc}}\right) \\
I_{NaBk_{sl}} &= F_{sl}\cdot G_{NaB}\cdot \left(V_m - E_{Na_{sl}}\right) \\
I_{NaBk} &= I_{NaBk_{junc}} + I_{NaBk_{sl}}
\end{aligned}
$$

A.2.4 $I_{Na,K}$: Na-K Pump Current

$$
\begin{aligned}
\sigma &= \frac{e^{\frac{Na_o}{67.3}} - 1}{7} \\
f_{NaK} &= \frac{1}{1 + 0.1245\cdot e^{-0.1\cdot V_m\cdot FoRT} + 0.0365\cdot \sigma\cdot e^{-V_m\cdot FoRT}} \\
I_{Na,K_{junc}} &= \frac{F_{junc}\cdot \bar{I}_{NaK}\cdot f_{NaK}\cdot K_o}{\left(1+\left(\frac{Km_{Naip}}{Na_j}\right)^4\right)\cdot (K_o + Km_{Ko})} \\
I_{Na,K_{sl}} &= \frac{F_{sl}\cdot \bar{I}_{NaK}\cdot f_{NaK}\cdot K_o}{\left(1+\left(\frac{Km_{Naip}}{Na_{sl}}\right)^4\right)\cdot (K_o + Km_{Ko})} \\
I_{Na,K} &= I_{Na,K_{junc}} + I_{Na,K_{sl}}
\end{aligned}
$$

A.2.5 I_{Kr}: Rapidly Activating Potassium Current

$$
\begin{aligned}
x_{r_{ss}} &= \frac{1}{1+e^{\frac{-(V_m+10)}{5}}} \\
\tau_{xr} &= \frac{3300}{\left(1+e^{\frac{-22-V_m}{9}}\right)\cdot\left(1+e^{\frac{V_m+11}{9}}\right)} + \frac{230}{1+e^{\frac{V_m+40}{20}}} \\
\frac{\mathrm{d}x_{Kr}}{\mathrm{d}t} &= \frac{x_{r_{ss}} - x_{Kr}}{\tau_{xr}} \\
r_{Kr} &= \frac{1}{1+e^{\frac{V_m+74}{24}}} \\
I_{Kr} &= G_{Kr}\cdot\sqrt{\frac{K_o}{5.4}}\cdot x_{Kr}\cdot r_{Kr}\cdot(V_m - E_K)
\end{aligned}
$$

A.2.6 I_{Ks}: Slowly Activating Potassium Current

$$
\begin{aligned}
x_{s_{ss}} &= \frac{1}{1+e^{\frac{-(V_m+3.8)}{14.25}}} \\
\tau_{xs} &= \frac{990.1}{1+e^{\frac{-(V_m+2.436)}{14.12}}} \\
\frac{\mathrm{d}x_{Ks}}{\mathrm{d}t} &= \frac{x_{s_{ss}} - x_{Ks}}{\tau_{xs}} \\
I_{Ks_{junc}} &= F_{junc}\cdot G_{Ks_{junc}}\cdot x_{Ks}^2\cdot(V_m - E_{Ks}) \\
I_{Ks_{sl}} &= F_{sl}\cdot G_{Ks_{sl}}\cdot x_{Ks}^2\cdot(V_m - E_{Ks}) \\
I_{Ks} &= I_{Ks_{junc}} + I_{Ks_{sl}}
\end{aligned}
$$

A.2.7 I_{Kp}: Plateau Potassium Current

$$
\begin{aligned}
kp_{Kp} &= \frac{1}{1+e^{7.488-\frac{V_m}{5.98}}} \\
I_{Kp} &= G_{Kp}\cdot kp_{Kp}\cdot(V_m - E_K)
\end{aligned}
$$

A.2.8 I_{to}: Transient Outward Potassium Current

$$
\begin{aligned}
x_{to_{ss}} &= \frac{1}{1+e^{\frac{-(V_m-19)}{13}}} \\
\tau_{x_{tos}} &= \frac{9}{1+e^{\frac{V_m+3}{15}}} + 0.5 \\
\frac{\mathrm{d}x_{to_s}}{\mathrm{d}t} &= \frac{x_{to_{ss}} - x_{to_s}}{\tau_{x_{tos}}} \\
y_{to_{ss}} &= \frac{1}{1+e^{\frac{V_m+19.5}{5}}} \\
\tau_{y_{tos}} &= \frac{800}{1+e^{\frac{V_m+60}{10}}} + 30 \\
\frac{\mathrm{d}y_{to_s}}{\mathrm{d}t} &= \frac{y_{to_{ss}} - y_{to_s}}{\tau_{y_{tos}}}
\end{aligned}
$$

$$\tau_{x_{tof}} = 8.5 \cdot e^{-\left(\frac{V_m+45}{50}\right)^2} + 0.5$$
$$\frac{dx_{to_f}}{dt} = \frac{x_{to_{ss}} - x_{to_f}}{\tau_{x_{tof}}}$$
$$\tau_{y_{tof}} = 85 \cdot e^{\frac{-(V_m+40)^2}{220}} + 7$$
$$\frac{dy_{to_f}}{dt} = \frac{y_{to_{ss}} - y_{to_f}}{\tau_{y_{tof}}}$$

$$I_{to_s} = G_{to_s} \cdot x_{to_s} \cdot y_{to_s} \cdot (V_m - E_K)$$
$$I_{to_f} = G_{to_f} \cdot x_{to_f} \cdot y_{to_f} \cdot (V_m - E_K)$$
$$I_{to} = I_{to_s} + I_{to_f}$$

A.2.9 I_{K1}:Inward Rectifier Potassium Current

$$a_{K1} = \frac{4.0938}{1 + e^{0.12165 \cdot (V_m - E_K - 49.9344)}}$$
$$b_{K1} = \frac{15.7197 \cdot e^{0.06739 \cdot (V_m - E_K - 3.2571)} + e^{0.06175 \cdot (V_m - E_K - 594.31)}}{1 + e^{-0.16285 \cdot (V_m - E_K + 14.2067)}}$$
$$K1_{ss} = \frac{a_{K1}}{a_{K1} + b_{K1}}$$
$$I_{K1} = G_{K1} \cdot \sqrt{\frac{K_o}{5.4}} \cdot K1_{ss} \cdot (V_m - E_K)$$

A.2.10 I_{ClCa}: Calcium-Activated Chlorine Current

$$I_{ClCa_{junc}} = \frac{F_{junc} \cdot G_{ClCa}}{1 + \frac{Kd_{ClCa}}{Ca_j}} \cdot (V_m - E_{Cl})$$
$$I_{ClCa_{sl}} = \frac{F_{sl} \cdot G_{ClCa}}{1 + \frac{Kd_{ClCa}}{Ca_{sl}}} \cdot (V_m - E_{Cl})$$
$$I_{ClCa} = I_{ClCa_{junc}} + I_{ClCa_{sl}}$$

A.2.11 I_{ClBk}: Background Chlorine Current

$$I_{ClBk} = G_{ClB} \cdot (V_m - E_{Cl})$$

A.2.12 I_{CaL}: L-type Calcium Current

Voltage-Dependent Activation Gate

$$
\begin{aligned}
d_{ss} &= \frac{1}{1+e^{\frac{-(V_m+5)}{6}}} \\
\alpha_d &= \frac{1.4}{1+e^{\frac{-35-V_m}{13}}} + 0.25 \\
\beta_d &= \frac{1.4}{1+e^{\frac{V_m+5}{5}}} \\
\gamma_d &= \frac{1}{1+e^{\frac{50-V_m}{20}}} \\
\tau_d &= \alpha_d \cdot \beta_d + \gamma_d \\
\frac{\mathrm{d}d}{\mathrm{d}t} &= \frac{d_{ss}-d}{\tau_d}
\end{aligned}
$$

Voltage-Dependent Inactivation Gates

$$
\begin{aligned}
f_{ss} &= \frac{1}{1+e^{\frac{V_m+20}{7}}} \\
\alpha_f &= 1102.5 \cdot e^{-\left(\frac{V_m+27}{15}\right)^2} \\
\beta_f &= \frac{200}{1+e^{\frac{13-V_m}{10}}} \\
\gamma_f &= \frac{180}{1+e^{\frac{V_m+30}{10}}} + 20 \\
\tau_f &= \alpha_f + \beta_f + \gamma_f \\
\frac{\mathrm{d}f}{\mathrm{d}t} &= \frac{f_{ss}-f}{\tau_f}
\end{aligned}
$$

$$
\begin{aligned}
f_{2_{ss}} &= \frac{0.67}{1+e^{\frac{V_m+35}{7}}} + 0.33 \\
\alpha_{f_2} &= 300 \cdot e^{\frac{-(V_m+25)^2}{170}} \\
\beta_{f_2} &= \frac{31}{1+e^{\frac{25-V_m}{10}}} \\
\gamma_{f_2} &= \frac{16}{1+e^{\frac{V_m+30}{10}}} \\
\tau_{f_2} &= \alpha_{f_2} + \beta_{f_2} + \gamma_{f_2} \\
\frac{\mathrm{d}f_2}{\mathrm{d}t} &= \frac{f_{2_{ss}}-f_2}{\tau_{f_2}}
\end{aligned}
$$

Calcium-Dependent Inactivation Gates

$$
\begin{aligned}
\frac{\mathrm{d}f_{Ca_{B_j}}}{\mathrm{d}t} &= 1.7 \cdot Ca_j \cdot \left(1-f_{Ca_{B_j}}\right) - 11.9 \cdot 10^{-3} \cdot f_{Ca_{B_j}} \\
\frac{\mathrm{d}f_{Ca_{B_{sl}}}}{\mathrm{d}t} &= 1.7 \cdot Ca_{sl} \cdot \left(1-f_{Ca_{B_{sl}}}\right) - 11.9 \cdot 10^{-3} \cdot f_{Ca_{B_{sl}}}
\end{aligned}
$$

Currents

$$\bar{I}_{Ca_j} = \frac{p_{Ca} \cdot V_m \cdot Frdy \cdot FoRT \cdot \left(Ca_j \cdot e^{2 \cdot V_m \cdot FoRT} - Ca_o\right)}{e^{2 \cdot V_m \cdot FoRT} - 1}$$
$$\bar{I}_{Ca_{sl}} = \frac{p_{Ca} \cdot V_m \cdot Frdy \cdot FoRT \cdot \left(Ca_{sl} \cdot e^{2 \cdot V_m \cdot FoRT} - Ca_o\right)}{e^{2 \cdot V_m \cdot FoRT} - 1}$$
$$\bar{I}_{Na_j} = \frac{p_{Na} \cdot V_m \cdot Frdy \cdot FoRT \cdot \left(Na_j \cdot e^{V_m \cdot FoRT} - Na_o\right)}{e^{V_m \cdot FoRT} - 1}$$
$$\bar{I}_{Na_{sl}} = \frac{p_{Na} \cdot V_m \cdot Frdy \cdot FoRT \cdot \left(Na_{sl} \cdot e^{V_m \cdot FoRT} - Na_o\right)}{e^{V_m \cdot FoRT} - 1}$$
$$\bar{I}_K = \frac{p_K \cdot V_m \cdot Frdy \cdot FoRT \cdot \left(K_i \cdot e^{V_m \cdot FoRT} - K_o\right)}{e^{V_m \cdot FoRT} - 1}$$

$$I_{Ca_{junc}} = F_{junc_{Ca_L}} \cdot \bar{I}_{Ca_j} \cdot d \cdot f \cdot f_2 \cdot \left(1 - f_{Ca_{B_j}}\right)$$
$$I_{Ca_{sl}} = F_{sl_{Ca_L}} \cdot \bar{I}_{Ca_{sl}} \cdot d \cdot f \cdot f_2 \cdot \left(1 - f_{Ca_{B_{sl}}}\right)$$
$$I_{CaNa_{junc}} = F_{junc_{Ca_L}} \cdot \bar{I}_{Na_j} \cdot d \cdot f \cdot f_2 \cdot \left(1 - f_{Ca_{B_j}}\right)$$
$$I_{CaNa_{sl}} = F_{sl_{Ca_L}} \cdot \bar{I}_{Na_{sl}} \cdot d \cdot f \cdot f_2 \cdot \left(1 - f_{Ca_{B_{sl}}}\right)$$
$$I_{CaK} = \bar{I}_K \cdot d \cdot f \cdot f_2 \cdot \left(F_{junc_{Ca_L}} \cdot \left(1 - f_{Ca_{B_j}}\right) + F_{sl_{Ca_L}} \cdot \left(1 - f_{Ca_{B_{sl}}}\right)\right)$$

$$I_{Ca} = I_{Ca_{junc}} + I_{Ca_{sl}}$$
$$I_{CaNa} = I_{CaNa_{junc}} + I_{CaNa_{sl}}$$
$$I_{CaL} = I_{Ca} + I_{CaK} + I_{CaNa}$$

A.2.13 I_{ncx}: Na-Ca Exchanger Current

$$
\begin{aligned}
Ka_{junc} &= \frac{1}{1+\left(\frac{Kd_{act}}{Ca_j}\right)^2} \\
Ka_{sl} &= \frac{1}{1+\left(\frac{Kd_{act}}{Ca_{sl}}\right)^2} \\
s1_{junc} &= e^{nu\cdot V_m\cdot FoRT}\cdot Na_j^3\cdot Ca_o \\
s1_{sl} &= e^{nu\cdot V_m\cdot FoRT}\cdot Na_{sl}^3\cdot Ca_o \\
s2_{junc} &= e^{(nu-1)\cdot V_m\cdot FoRT}\cdot Na_o^3\cdot Ca_j \\
s2_{sl} &= e^{(nu-1)\cdot V_m\cdot FoRT}\cdot Na_o^3\cdot Ca_{sl} \\
s3_{junc} &= Km_{Ca_i}\cdot Na_o^3\cdot\left(1+\left(\frac{Na_j}{Km_{Na_i}}\right)^3\right)+Km_{Na_o}^3\cdot Ca_j\cdot\left(1+\frac{Ca_j}{Km_{Ca_i}}\right) \\
&\quad + Km_{Ca_o}\cdot Na_j^3+Na_j^3\cdot Ca_o+Na_o^3\cdot Ca_j \\
s3_{sl} &= Km_{Ca_i}\cdot Na_o^3\cdot\left(1+\left(\frac{Na_{sl}}{Km_{Na_i}}\right)^3\right)+Km_{Na_o}^3\cdot Ca_{sl}\cdot\left(1+\frac{Ca_{sl}}{Km_{Ca_i}}\right) \\
&\quad + Km_{Ca_o}\cdot Na_{sl}^3+Na_{sl}^3\cdot Ca_o+Na_o^3\cdot Ca_{sl}
\end{aligned}
$$

$$
\begin{aligned}
I_{ncx_{junc}} &= \frac{F_{junc}\cdot\bar{I}_{NCX}\cdot Ka_{junc}\cdot(s1_{junc}-s2_{junc})}{s3_{junc}\cdot\left(1+k_{sat}\cdot e^{(nu-1)\cdot V_m\cdot FoRT}\right)} \\
I_{ncx_{sl}} &= \frac{F_{sl}\cdot\bar{I}_{NCX}\cdot Ka_{sl}\cdot(s1_{sl}-s2_{sl})}{s3_{sl}\cdot\left(1+k_{sat}\cdot e^{(nu-1)\cdot V_m\cdot FoRT}\right)} \\
I_{ncx} &= I_{ncx_{junc}}+I_{ncx_{sl}}
\end{aligned}
$$

A.2.14 I_{pCa}: Sarcolemmal Calcium Pump Current

$$
\begin{aligned}
I_{pCa_{junc}} &= \frac{F_{junc}\cdot\bar{I}_{PMCA}\cdot Ca_j^{1.6}}{Km_{pCa}^{1.6}+Ca_j^{1.6}} \\
I_{pCa_{sl}} &= \frac{F_{sl}\cdot\bar{I}_{PMCA}\cdot Ca_{sl}^{1.6}}{Km_{pCa}^{1.6}+Ca_{sl}^{1.6}} \\
I_{pCa} &= I_{pCa_{junc}}+I_{pCa_{sl}}
\end{aligned}
$$

A.2.15 I_{CaBk}: Background Calcium Current

$$
\begin{aligned}
I_{CaBk_{junc}} &= F_{junc}\cdot G_{CaB}\cdot\left(V_m-E_{Ca_{junc}}\right) \\
I_{CaBk_{sl}} &= F_{sl}\cdot G_{CaB}\cdot\left(V_m-E_{Ca_{sl}}\right) \\
I_{CaBk} &= I_{CaBk_{junc}}+I_{CaBk_{sl}}
\end{aligned}
$$

A.2.16 SR Fluxes: Calcium Release, SR Calcium Pump, SR Calcium Leak

$$
\begin{aligned}
k_{Ca_{SR}} &= Max_{SR} - \frac{Max_{SR} - Min_{SR}}{1 + \left(\frac{ec50_{SR}}{Ca_{SR}}\right)^{2.5}} \\
ko_{SR_{Ca}} &= \frac{ko_{Ca}}{k_{Ca_{SR}}} \\
ki_{SR_{Ca}} &= ki_{Ca} \cdot k_{Ca_{SR}} \\
RI &= 1 - Ry_{Rr} - Ry_{Ro} - Ry_{Ri} \\
\frac{\mathrm{d}Ry_{Rr}}{\mathrm{d}t} &= ki_m \cdot RI - ki_{SR_{Ca}} \cdot Ca_j \cdot Ry_{Rr} - \left(ko_{SR_{Ca}} \cdot Ca_j^2 \cdot Ry_{Rr} - ko_m \cdot Ry_{Ro}\right) \\
\frac{\mathrm{d}Ry_{Ro}}{\mathrm{d}t} &= ko_{SR_{Ca}} \cdot Ca_j^2 \cdot Ry_{Rr} - ko_m \cdot Ry_{Ro} - (ki_{SR_{Ca}} \cdot Ca_j \cdot Ry_{Ro} - ki_m \cdot Ry_{Ri}) \\
\frac{\mathrm{d}Ry_{Ri}}{\mathrm{d}t} &= ki_{SR_{Ca}} \cdot Ca_j \cdot Ry_{Ro} - ki_m \cdot Ry_{Ri} - \left(ko_m \cdot Ry_{Ri} - ko_{SR_{Ca}} \cdot Ca_j^2 \cdot RI\right) \\
J_{SR_{Ca_{rel}}} &= ks \cdot Ry_{Ro} \cdot (Ca_{SR} - Ca_j) \\
J_{ser_{Ca}} &= \frac{V_{max_{SR_{CaP}}} \cdot \left(\left(\frac{Ca_i}{Km_f}\right)^{hill_{SR_{CaP}}} - \left(\frac{Ca_{SR}}{Km_r}\right)^{hill_{SR_{CaP}}}\right)}{1 + \left(\frac{Ca_i}{Km_f}\right)^{hill_{SR_{CaP}}} + \left(\frac{Ca_{SR}}{Km_r}\right)^{hill_{SR_{CaP}}}} \\
J_{SR_{leak}} &= 5.348 \cdot 10^{-6} \cdot (Ca_{SR} - Ca_j)
\end{aligned}
$$

A.2.17 Ion Homeostasis

Sodium Buffers

$$
\begin{aligned}
\frac{\mathrm{d}Na_{B_j}}{\mathrm{d}t} &= k_{on_{Na}} \cdot Na_j \cdot \left(B_{max_{Na_j}} - Na_{B_j}\right) - k_{off_{Na}} \cdot Na_{B_j} \\
\frac{\mathrm{d}Na_{B_{sl}}}{\mathrm{d}t} &= k_{on_{Na}} \cdot Na_{sl} \cdot \left(B_{max_{Na_{sl}}} - Na_{B_{sl}}\right) - k_{off_{Na}} \cdot Na_{B_{sl}}
\end{aligned}
$$

Cytosolic Calcium Buffers

$$\frac{\mathrm{d}TnC_l}{\mathrm{d}t} = k_{on_{TnC_l}} \cdot Ca_i \cdot \left(B_{max_{TnC_{low}}} - TnC_l\right) - k_{off_{TnC_l}} \cdot TnC_l$$
$$\frac{\mathrm{d}TnC_{h_c}}{\mathrm{d}t} = k_{on_{TnC_{h_{Ca}}}} \cdot Ca_i \cdot \left(B_{max_{TnC_{high}}} - TnC_{h_c} - TnC_{h_m}\right) - k_{off_{TnC_{h_{Ca}}}} \cdot TnC_{h_c}$$
$$\frac{\mathrm{d}TnC_{h_m}}{\mathrm{d}t} = k_{on_{TnC_{h_{Mg}}}} \cdot Mg_i \cdot \left(B_{max_{TnC_{high}}} - TnC_{h_c} - TnC_{h_m}\right) - k_{off_{TnC_{h_{Mg}}}} \cdot TnC_{h_m}$$
$$\frac{\mathrm{d}CaM}{\mathrm{d}t} = k_{on_{CaM}} \cdot Ca_i \cdot (B_{max_{CaM}} - CaM) - k_{off_{CaM}} \cdot CaM$$
$$\frac{\mathrm{d}Myo_c}{\mathrm{d}t} = k_{on_{myo_{Ca}}} \cdot Ca_i \cdot \left(B_{max_{myosin}} - Myo_c - Myo_m\right) - k_{off_{myo_{Ca}}} \cdot Myo_c$$
$$\frac{\mathrm{d}Myo_m}{\mathrm{d}t} = k_{on_{myo_{Mg}}} \cdot Mg_i \cdot \left(B_{max_{myosin}} - Myo_c - Myo_m\right) - k_{off_{myo_{Mg}}} \cdot Myo_m$$
$$\frac{\mathrm{d}SRB}{\mathrm{d}t} = k_{on_{SR}} \cdot Ca_i \cdot (B_{max_{SR}} - SRB) - k_{off_{SR}} \cdot SRB$$
$$J_{Ca_{B_{cytosol}}} = \frac{\mathrm{d}TnC_l}{\mathrm{d}t} + \frac{\mathrm{d}TnC_{h_c}}{\mathrm{d}t} + \frac{\mathrm{d}TnC_{h_m}}{\mathrm{d}t} + \frac{\mathrm{d}CaM}{\mathrm{d}t} + \frac{\mathrm{d}Myo_c}{\mathrm{d}t} + \frac{\mathrm{d}Myo_m}{\mathrm{d}t} + \frac{\mathrm{d}SRB}{\mathrm{d}t}$$

Junctional and SL Calcium Buffers

$$\frac{\mathrm{d}SLL_j}{\mathrm{d}t} = k_{on_{sl_l}} \cdot Ca_j \cdot \left(B_{max_{SL_{low_j}}} - SLL_j\right) - k_{off_{sl_l}} \cdot SLL_j$$
$$\frac{\mathrm{d}SLL_{sl}}{\mathrm{d}t} = k_{on_{sl_l}} \cdot Ca_{sl} \cdot \left(B_{max_{SL_{low_{sl}}}} - SLL_{sl}\right) - k_{off_{sl_l}} \cdot SLL_{sl}$$
$$\frac{\mathrm{d}SLH_j}{\mathrm{d}t} = k_{on_{sl_h}} \cdot Ca_j \cdot \left(B_{max_{SL_{high_j}}} - SLH_j\right) - k_{off_{sl_h}} \cdot SLH_j$$
$$\frac{\mathrm{d}SLH_{sl}}{\mathrm{d}t} = k_{on_{sl_h}} \cdot Ca_{sl} \cdot \left(B_{max_{SL_{high_{sl}}}} - SLH_{sl}\right) - k_{off_{sl_h}} \cdot SLH_{sl}$$
$$J_{Ca_{B_{junction}}} = \frac{\mathrm{d}SLL_j}{\mathrm{d}t} + \frac{\mathrm{d}SLH_j}{\mathrm{d}t}$$
$$J_{Ca_{B_{sk}}} = \frac{\mathrm{d}SLL_{sl}}{\mathrm{d}t} + \frac{\mathrm{d}SLH_{sl}}{\mathrm{d}t}$$

Sodium Concentrations

$$\frac{\mathrm{d}Na_j}{\mathrm{d}t} = \frac{-I_{Na_{tot_{junc}}} \cdot C_{mem}}{V_{junc} \cdot Frdy} + \frac{J_{Na_{junc,sl}}}{V_{junc}} \cdot (Na_{sl} - Na_j) - \frac{\mathrm{d}Na_{B_j}}{\mathrm{d}t}$$
$$\frac{\mathrm{d}Na_{sl}}{\mathrm{d}t} = \frac{-I_{Na_{tot_{sl}}} \cdot C_{mem}}{V_{sl} \cdot Frdy} + \frac{J_{Na_{junc,sl}}}{V_{sl}} \cdot (Na_j - Na_{sl}) + \frac{J_{Na_{sl,myo}}}{V_{sl}} \cdot (Na_i - Na_{sl}) - \frac{\mathrm{d}Na_{B_{sl}}}{\mathrm{d}t}$$
$$\frac{\mathrm{d}Na_i}{\mathrm{d}t} = \frac{J_{Na_{sl,myo}}}{V_{myo}} \cdot (Na_{sl} - Na_i)$$

Calcium Concentrations

$$\frac{\mathrm{d}Csqn_b}{\mathrm{d}t} = k_{on_{csqn}} \cdot Ca_{SR} \cdot \left(B_{max_{csqn}} - Csqn_b\right) - k_{off_{csqn}} \cdot Csqn_b$$
$$\frac{\mathrm{d}Ca_j}{\mathrm{d}t} = \frac{-I_{Catot_{junc}} \cdot C_{mem}}{V_{junc} \cdot 2 \cdot Frdy} + \frac{J_{Cajunc,sl}}{V_{junc}} \cdot (Ca_{sl} - Ca_j) - J_{CaB_{junction}} + \frac{J_{SRCa_{rel}} \cdot V_{sr}}{V_{junc}} + \frac{J_{SRleak} \cdot V_{myo}}{V_{junc}}$$
$$\frac{\mathrm{d}Ca_{sl}}{\mathrm{d}t} = \frac{-I_{Catot_{sl}} \cdot C_{mem}}{V_{sl} \cdot 2 \cdot Frdy} + \frac{J_{Cajunc,sl}}{V_{sl}} \cdot (Ca_j - Ca_{sl}) + \frac{J_{Ca_{sl,myo}}}{V_{sl}} \cdot (Ca_i - Ca_{sl}) - J_{CaB_{sk}}$$
$$\frac{\mathrm{d}Ca_i}{\mathrm{d}t} = \frac{-J_{ser_{Ca}} \cdot V_{sr}}{V_{myo}} - J_{CaB_{cytosol}} + \frac{J_{Ca_{sl,myo}}}{V_{myo}} \cdot (Ca_{sl} - Ca_i)$$
$$\frac{\mathrm{d}Ca_{SR}}{\mathrm{d}t} = J_{ser_{Ca}} - \left(\frac{J_{SRleak} \cdot V_{myo}}{V_{sr}} + J_{SRCa_{rel}}\right) - \frac{\mathrm{d}Csqn_b}{\mathrm{d}t}$$

A.2.18 Membrane Potential

$$I_{Catot_{junc}} = I_{Cajunc} + I_{CaBkjunc} + I_{pCa_{junc}} - 2 \cdot I_{ncx_{junc}}$$
$$I_{Catot_{sl}} = I_{Ca_{sl}} + I_{CaBk_{sl}} + I_{pCa_{sl}} - 2 \cdot I_{ncx_{sl}}$$
$$I_{Catot} = I_{Catot_{junc}} + I_{Catot_{sl}}$$

$$I_{K_{tot}} = I_{to} + I_{Kr} + I_{Ks} + I_{K1} - 2 \cdot I_{Na,K} + I_{Ca_K} + I_{Kp}$$

$$I_{Natot_{junc}} = I_{Na_{junc}} + I_{NaBk_{junc}} + 3 \cdot I_{ncx_{junc}} + 3 \cdot I_{Na,K_{junc}} + I_{CaNa_{junc}}$$
$$I_{Natot_{sl}} = I_{Na_{sl}} + I_{NaBk_{sl}} + 3 \cdot I_{ncx_{sl}} + 3 \cdot I_{Na,K_{sl}} + I_{CaNa_{sl}}$$
$$I_{Natot} = I_{Natot_{junc}} + I_{Natot_{sl}}$$

$$I_{Cl_{tot}} = I_{ClCa} + I_{ClBk}$$

$$I_{ion} = I_{Na_{tot}} + I_{Cl_{tot}} + I_{Ca_{tot}} + I_{K_{tot}}$$
$$\frac{\mathrm{d}V_m}{\mathrm{d}t} = -\left(I_{ion} - I_{stim}\right)$$

A.3 Initial Conditions

Name	EPI	ENDO	Units
Ca_{SR}	$6.093596 \cdot 10^{-1}$	$6.138856 \cdot 10^{-1}$	mM
Ca_i	$9.658067 \cdot 10^{-5}$	$9.719632 \cdot 10^{-5}$	mM
Ca_j	$2.038197 \cdot 10^{-4}$	$2.048633 \cdot 10^{-4}$	mM
Ca_{sl}	$1.184305 \cdot 10^{-4}$	$1.188246 \cdot 10^{-4}$	mM
$Csqn_b$	1.258048	1.262853	mM
CaM	$3.267494 \cdot 10^{-4}$	$3.288063 \cdot 10^{-4}$	mM
Myo_c	$2.520383 \cdot 10^{-3}$	$2.522168 \cdot 10^{-3}$	mM
Myo_m	$1.369529 \cdot 10^{-1}$	$1.369514 \cdot 10^{-1}$	mM
SRB	$2.373753 \cdot 10^{-3}$	$2.38683 \cdot 10^{-3}$	mM
TnC_{h_c}	$1.225914 \cdot 10^{-1}$	$1.225802 \cdot 10^{-1}$	mM
TnC_{h_m}	$8.12201 \cdot 10^{-3}$	$8.128604 \cdot 10^{-3}$	mM
TnC_l	$9.757237 \cdot 10^{-3}$	$9.811535 \cdot 10^{-3}$	mM
h	$7.13497 \cdot 10^{-1}$	$7.126555 \cdot 10^{-1}$	$[-]$
j	$7.128671 \cdot 10^{-1}$	$7.119893 \cdot 10^{-1}$	$[-]$
m	$2.163678 \cdot 10^{-3}$	$2.176608 \cdot 10^{-3}$	$[-]$
SLH_j	$8.053908 \cdot 10^{-2}$	$8.078504 \cdot 10^{-2}$	mM
SLH_{sl}	$1.235381 \cdot 10^{-1}$	$1.238366 \cdot 10^{-1}$	mM
SLL_j	$8.563314 \cdot 10^{-3}$	$8.606485 \cdot 10^{-3}$	mM
SLL_{sl}	$1.097424 \cdot 10^{-2}$	$1.101044 \cdot 10^{-2}$	mM
d	$1.871177 \cdot 10^{-6}$	$1.879996 \cdot 10^{-6}$	$[-]$
f	$9.804391 \cdot 10^{-1}$	$9.789409 \cdot 10^{-1}$	$[-]$
f_2	$9.99401 \cdot 10^{-1}$	$9.993986 \cdot 10^{-1}$	$[-]$
f_{CaB_j}	$2.847118 \cdot 10^{-2}$	$2.861794 \cdot 10^{-2}$	$[-]$
$f_{CaB_{sl}}$	$1.692189 \cdot 10^{-2}$	$1.69833 \cdot 10^{-2}$	$[-]$
x_{Kr}	$1.516232 \cdot 10^{-2}$	$1.896559 \cdot 10^{-2}$	$[-]$
Ry_{Ri}	$1.411382 \cdot 10^{-7}$	$1.43831 \cdot 10^{-7}$	$[-]$
Ry_{Ro}	$1.126209 \cdot 10^{-6}$	$1.149876 \cdot 10^{-6}$	$[-]$
Ry_{Rr}	$8.886338 \cdot 10^{-1}$	$8.888214 \cdot 10^{-1}$	$[-]$
x_{Ks}	$3.549354 \cdot 10^{-3}$	$3.55636 \cdot 10^{-3}$	$[-]$
Na_{B_j}	3.796195	3.785209	mM
$Na_{B_{sl}}$	$8.283308 \cdot 10^{-1}$	$8.259271 \cdot 10^{-1}$	mM
Na_i	$1.007825 \cdot 10^{1}$	$1.001989 \cdot 10^{1}$	mM
Na_j	$1.007931 \cdot 10^{1}$	$1.00211 \cdot 10^{1}$	mM
Na_{sl}	$1.00781 \cdot 10^{1}$	$1.001974 \cdot 10^{1}$	mM
x_{to_f}	$3.584625 \cdot 10^{-4}$	$3.592405 \cdot 10^{-4}$	$[-]$
x_{to_s}	$3.584727 \cdot 10^{-4}$	$3.592503 \cdot 10^{-4}$	$[-]$
y_{to_f}	$9.999976 \cdot 10^{-1}$	$9.999976 \cdot 10^{-1}$	$[-]$
y_{to_s}	$8.087629 \cdot 10^{-1}$	$8.161309 \cdot 10^{-1}$	$[-]$
V_m	-84.13368	-84.10546	mV

Appendix B

International Conferences

B.1 Computing in Cardiology 2010, Belfast (United Kingdom)

Analysis and Improvement of a Human Ventricular Cell Model for Investigation of Cardiac Arrhythmias

J Carro[1,2], JF Rodríguez[1], P Laguna[1,2], E Pueyo[1,2]

[1]Instituto de Investigación en Ingeniería de Aragón (I3A), Universidad de Zaragoza, Spain
[2]CIBER de Bioingeniería, Biomateriales y Nanomedicina (CIBER-BBN), Spain

Abstract

The use of experiments for studying cardiac arrhythmias, the effect of drugs, or pathologies on cardiac electrophysiology is very limited. This has made mathematical modeling and simulation of heart's electrical activity a fundamental tool to understand cardiac behavior. In this study several modifications were introduced to a recently proposed human ventricular cell model. Four stimulation protocols were applied to the original and improved models of isolated cell, and a number of cellular arrhythmic risk biomarkers were computed: steady-state action potential (AP) and $[Ca^{2+}]$ *transient properties, AP duration (APD) restitution curves, APD adaptation to abrupt changes in heart rate, and intracellular* $[Ca^{2+}]$ *and* $[Na^{+}]$ *rate dependence. Our modifications led to: a) further improved AP triangulation (*$78.1\ ms$*); b) APD rate adaptation curves characterized by fast and slow time constants within physiological ranges (*$10.1\ s$ *and* $105.9\ s$*); c) maximum S1S2 restitution slope in accordance with experimental data (*$S_{S1S2} = 1.0$*).*

1. Introduction

Ventricular arrhythmias can have their origin in diseases, genetic disorders, drug cardiotoxicity, and a number of other causes. Research in this field has identified a number of potential biomarkers of arrhythmic risk related to cellular electrophysiological properties. However, performing experimental and clinical studies involving human hearts to quantify these biomarkers is very difficult. On the other hand, animal hearts used for experimental studies may differ significantly from human hearts. In addition, ventricular cardiac arrhythmias are three-dimensional phenomena whereas experimental observations are still largely constrained to surface recordings. Under this circumstances, mathematical models of myocardial cells and computer simulations of cardiac activity in the human heart can overcome some of these problems.

Recently, a new model has been proposed by Grandi et al. [1] (GR) that improves the response to frequency changes and has a better performance against current blocks with respect to the model proposed by ten Tusscher and Panfilov [2] (TTP06). This article introduces several modifications to the GR model by accounting for recent experimental measurements of potassium currents [3] and the introduction of fast and slow inactivation of L-type calcium current [2]. The performance of the proposed model, herein denoted by CRR, has been tested against the GR and TTP06 models by applying four stimulation protocols and computing twelve cellular arrhythmic risk biomarkers following the methodology proposed in [4]. The results show that the introduced modifications have brought most biomarkers into the physiological range, and considerably improved others with respect to the GR and TTP06 models of AP.

2. Methods

2.1. Biomarkers of arrhythmic risk

Four stimulation protocols have been applied and twelve cellular biomarkers of arrhythmic risk have been computed as in [4]:

Steady-state AP and intracellular $[Ca^{2+}]$ *concentration properties*. Systolic and diastolic $[Ca^{2+}]_i$ levels under steady-state pacing at frequencies of 0.5 and 1 Hz and APD and AP Triangulation at 1 Hz have been calculated. These biomarkers have been proposed as arrhythmic risk biomarkers in the literature [5–7].

APD restitution (APDR) curves. APDR curves have been obtained using the S1S2 and the dynamic restitution protocols as in [4]. In both cases, the maximum slope, suggested as a risk marker in the literature [8, 9], has been computed.

APD rate adaptation to abrupt changes in cycle length (CL). APD rate adaptation dynamics have been proposed as a clinical marker in [10]. Dynamics have been fitted to two exponentials with time constants τ_{fast} and τ_{slow} [11].

Rate dependence of steady-state $[Na^{+}]_i$ *and* $[Ca^{2+}]_i$.

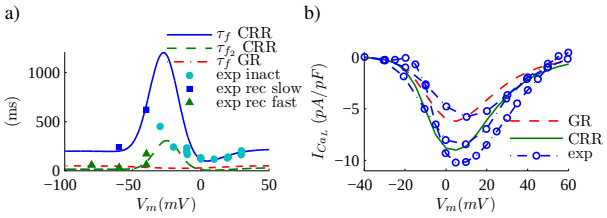

Figure 1. *I_{Ca_L} characteristics in simulations and experiments:* a) Inactivation time constants; b) current density versus voltage. Markers: experimental data.

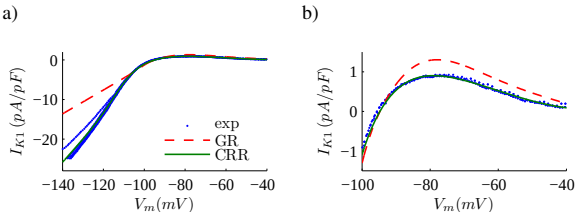

Figure 2. Maximum I_{K1} versus voltage and experimental data. $[K^+]_i = 138\ mM$ and $[K^+]_o = 4\ mM$. Blue dots: experimental data.

The importance of $[Na^+]_i$ and $[Ca^{2+}]_i$ dynamics in arrhythmogenesis has been reported [12, 13]. The systolic values of both concentrations have been measured at different frequencies (0.25, 0.5, 1, 1.5, 2, 2.5 and 3 Hz) and normalized to the level of the minimum frequency. The maximum value has been computed and used as biomarker.

2.2. Modifications of the model

Two ionic currents have been reformulated and some model parameters have been redefined in the GR model:

L-Type Calcium Current (I_{Ca_L}). The voltage-dependent inactivation gate f has been replaced with the product of a fast, f, and a slow, f_2, inactivation gates as in [2]. Based on available experimental data, the value of the opening rate α_{f_2}, associated with f_2, has been modified to:

$$\alpha_{f_2} = 300 \cdot e^{-\frac{(V_m+25)^2}{170}},$$

where V_m denotes the transmembrane potential.

Figure 1a depicts τ_f and τ_{f_2} along with experimental data [2].The time constant (τ_d) of the activation gate d has been replaced with the description given in [2]. The relative permeabilities of the L-type calcium channels have been adjusted to: $p_{Ca} = 1.458 \cdot 10^{-4}\ cm/s$, $p_K = 7.290 \cdot 10^{-8}\ cm/s$, $p_{Na} = 4.050 \cdot 10^{-9}\ cm/s$.

This new definition of I_{Ca_L} is compared against experimental data and the original definition of the GR model in Figure 1b. Experimental data is from [14–16].

Inward Rectifier K Current (I_{K1}). This current has been re-adjusted based on experimental data from [3]. The re-adjusted current is formulated as follows:

$$V_{E_k} = V_m - E_k$$

$$a_{K1} = \frac{4.094}{1.0 + e^{0.1217 \cdot (V_{E_k} - 49.934)}}$$

$$b_{K1} = \frac{15.720 \cdot e^{0.0674 \cdot (V_{E_k} - 3.257)} + e^{0.0618 \cdot (V_{E_k} - 594.31)}}{1.0 + e^{-0.1629 \cdot (V_{E_k} + 14.207)}}$$

$$K1_{ss} = \frac{a_{K1}}{a_{K1} + b_{K1}}$$

$$I_{K1} = 0.5715 \cdot \sqrt{\frac{[K^+]_o}{5.4}} \cdot K1_{ss} \cdot V_{E_k}$$

where $[K^+]_o$ denotes the extracellular K^+ concentration, and E_K is the K^+ reversal potential. Figure 2 shows the modified I_{K1} compared against the experimental data from [3] and I_{K1} from the GR model. Note that Figure 2b is a zoom from Figure 2a.

$I_{Na,K}$: Na/K Pump Current. Maximal $I_{Na,K}$ conductance has been reduced by 45%.

$[K^+]_i$ and G_{Na}. A more physiological value of $[K^+]_i$ ($138\ mM$) has been used in the model. In this regard, in order to get physiological values for the maximal upstroke velocity, dV/dt, the maximum conductance of the sodium current, G_{Na}, has been reduced to $18.86\ mS/\mu F$.

2.3. Blocking Currents

We have also studied the behavior of the model under total and partial block of potassium currents, comparing the results against those reported in [17]:

I_{Ks}: To simulate the effect of $1\ \mu M$ of HMR-1556, I_{Ks} has been completely blocked.

I_{Kr}: To simulate the effect of $50\ nM$ of dofetilide, I_{Kr} has been completely blocked.

I_{K1}: To simulate the effect of $10\ \mu M$ of $BaCl_2$, I_{K1} has been blocked at 50%.

2.4. Numerical implementation and simulation

Model differential equations were implemented in Fortran. Cells were stimulated with square transmembrane current pulses twice the diastolic threshold at CL = 1000 ms and 1-ms duration. Forward Euler integration with a time step $\Delta t = 0.002\ ms$ was used to integrate the system of differential equations governing the cellular electrical behavior. The Rush and Larsen integration scheme was used to integrate the Hodgkin-Huxley type equations for the gating variables of the various time-dependent currents.

Biomarker	TTP06	GR	CRR	Physiolo.
APD_{90}	301.2	285.0	306.1	271-366
Triangulation	28.4	51.5	78.1	44-112
Sys $[Ca^{2+}]_i$ 1 Hz	0.886	0.383	0.602	1.59-2.01
Sys $[Ca^{2+}]_i$ 0.5 Hz	0.199	0.345	0.522	0.71-1.68
Dia $[Ca^{2+}]_i$ 1 HZ	0.104	0.089	0.097	0.20-0.33
Dia $[Ca^{2+}]_i$ 0.5 Hz	0.068	0.085	0.091	0.14-0.32
$S_{max_{S1S2}}$	1.3	0.2	1.0	0.79-4.25
$S_{max_{DYN}}$	1.0	1.1	0.9	—
τ_{fast}	13.3	—	10.1	—
τ_{slow}	124.8	56.3	105.9	70-110
Max. sys. $[Ca^{2+}]_i$	1157	178	147	130-170
Max. sys. $[Na^{+}]_i$	217	132	134	145

Table 1. Biomarkers of arrhythmic risk for the TTP06, GR and CRR human models. Green color indicates within physiological range. Blue color indicates out of physiological range but better than previous models. Red color indicates out of physiological range.

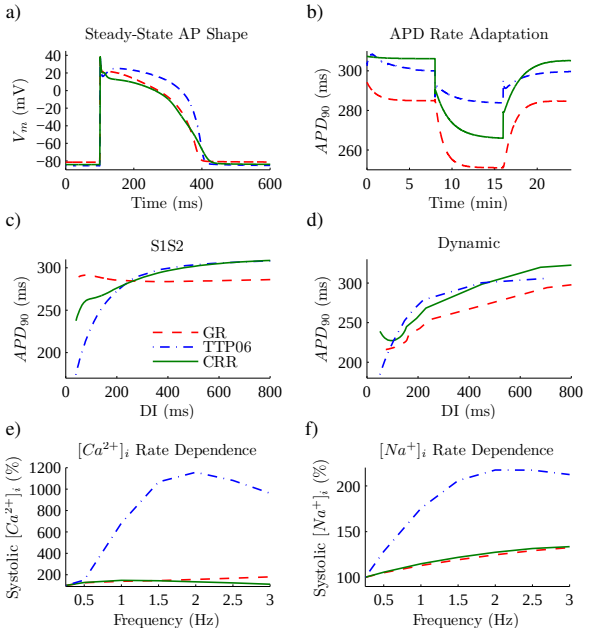

Figure 3. Biomarkers of arrhythmic risk from TTP06, GR and CRR models: a) AP for CL = 1000 ms; b) APD rate adaptation to abrupt changes in CL (From 1000 ms to 600 ms); c) S1S2 restitution protocol curve; d) Dynamic restitution protocol curve; e) rate dependence of steady-state $[Na^{+}]_i$; f) rate dependence of steady-state $[Ca^{2+}]_i$

3. Results

3.1. Biomarkers of arrhythmic risk

Table 1 shows the computed biomarkers for the modified model, CRR. Results are compared against those obtained with previous models (TTP06 and GR) and against a variety of physiological data described in [4].

These results indicate that the GR model performs better than the TTP06 model, with respect to the following biomarkers: triangulation, systolic and diastolic $[Ca^{2+}]_i$ at 0.5 Hz and rate dependence of steady-state $[Na^{+}]_i$ and $[Ca^{2+}]_i$. However, according to other analyzed biomarkers, the GR model renders worse results than the TTP06 model. Particularly, in [18] two phases of APD rate adaptation curve were reported: a first phase with a rapid time constant and a second phase with a slower time constant. The GR model does not present this first phase. Also, the S1S2 restitution curves of the TTP06 model (Figure 3c) are in better agreement with experimental data.

For the CRR model, most of the twelve analyzed biomarkers are within the physiological range or otherwise closer to the physiological range as compared to GR and TTP06 models, except for systolic and diastolic $[Ca^{2+}]_i$ levels at 0.5 Hz where TTP06 outperforms CRR.

3.2. Blocking Currents

Table 2 summarizes the effect of current block on the different models. Results are given as percentage of variation of the APD value in control conditions. In those cases where more than one current is blocked, the variation refers to the APD obtained when the first current is blocked. Experimental values have been taken from [17].

4. Discussion and conclusions

This study introduces several modifications to the GR model by accounting for recent experimental measurements of potassium currents, and by reformulating the L-type calcium current so as to introduce fast and slow voltage-dependent inactivation. All the modifications have been made with the aim of maintaining the advantages that the GR model presents over previous models while improving the performance on other electrophysiological aspects.

For the proposed CRR model, the introduction of fast and slow I_{CaL} inactivation has led to a more physiological rate adaptation response as compared to the original GR model. The other modifications have rendered most biomarkers to be within the physiological range or otherwise closer to the physiological range as compared to the GR and TTP06 models, except for systolic and diastolic $[Ca^{2+}]_i$ levels at 0.5 Hz where TTP06 outperforms CRR. These modifications, however, have altered the behavior of the model against current blocks minimally.

The results of the analysis conducted in this study points out the importance that calcium dynamics have over differ-

Current		Ref.	TT	GR	CRR	Exper.
I_{Kr}	0%	Control	74.9	0.7	0.6	< 2.8
I_{Kr}	0%	Control	15.9	18.6	14.1	44±4
I_{Ks} I_{Kr}	0% 0%	I_{Kr} B.	—	1.4	0.8	9
I_{K1}	50%	Control	3.6	11.5	14.6	4.8±1.5
I_{Kr} I_{K1}	0% 50%	I_{Kr} B.	8.9	15.6	21.1	33

Table 2. Percentages of variation in the APD caused by blocking different currents. Green color indicates within physiological range. Blue color indicates out of physiological range but better than previous models. Red color indicate out of physiological range.

ent biomarkers. This suggests the need for continuing with the development of more reliable calcium dynamic models that allow improving the performance of whole cell AP models.

Further developments of the proposed model will include conducting a sensitivity analysis of the studied biomarkers to changes in model parameters as proposed in [4], as well as testing the performance of the model under pathological conditions such as hyperkalemia.

Acknowledgements

This study was financially supported by grants TEC2007-68076-C02-02 from Ministerio de Ciencia e Innovación, Spain, and PI144/2009 from Gobierno de Aragón, Spain, and fellowship B040/2010 from Gobierno de Aragón, Spain.

References

[1] Grandi E, Pasqualini FS, Bers DM. A novel computational model of the human ventricular action potential and ca transient. J Mol Cell Cardiol 2010;48:112 – 121.

[2] ten Tusscher K, Panfilov A. Alternans and spiral breakup in a human ventricular tissue model. Am J Physiol Heart Circ Physiol 2006;291:H1088–H1100.

[3] Fink M, Noble D, Virag L, Varro A, Giles WR. Contributions of herg k+ current to repolarization of the human ventricular action potential. Progress in Biophysics and Molecular Biology 2008;96:357 – 376. ISSN 0079-6107.

[4] Romero L, Pueyo E, Fink M, Rodríguez B. Impact of ionic current variability on human ventricular cellular electrophysiology. Am J Physiol Heart Circ Physiol 2009; 297:H1436–1445.

[5] Bers DM, Despa S. Cardiac myocytes ca2+ and na+ regulation in normal and failing hearts. J Pharm Sci 2006; 100:315–322.

[6] Hondeghem L, Carlsson L, Duker G. Instability and triangulation of the action potential preict serious proarrhythmia, but action potential duration prolongation is antiarrhythmic. Circ 2001;103:2004–2013.

[7] Volders P, Vos M, Szabo B, Sipido K, de Groot S, Gorgels A, Wellens H, Lazzara R. Progress in the understanding of cardiac early afterdepolarizations and torsades de pointes: time to revise current concepts. Cardiovasc Res 2000; 46:376–392.

[8] Nolasco J, Dahlen R. A graphic method for the study of alternation in cardiac action potentials. J Appl Physiol 1968; 25:191–196.

[9] Weiss J, Karma A, Shiferaw U, Chen P, Garfinkel A, Qu Z. From pulses to pulseless: the saga of cardiac alternans. Circ Res 2006;98:1244–1253.

[10] Pueyo E, Smetana P, Caminal P, de Luna A, Malik M, Laguna P. Characterization of qt interval adaptation to rr interval changes and its use as a risk-stratifier of arrhythmic mortality in amiodarone-treated survivors of acute myocardial infarction. IEEE Trans Biomed Eng 2004;51:1511–1520.

[11] Pueyo E, Husti Z, Hornyik T, Baczkó I, Laguna P, Varró A, Rodríguez B. Mechanisms of ventricular rate adaptation as a predictor of arrhythmic risk. Am J Physiol Heart Circ Physiol 2010;298:H1577–H1587.

[12] Levi A, Dalton G, Hancox J, Mitcheson J, Issberner J, Bates J, Evans S, Howarth F, Hobai I, Jones J. Role of intracellular sodium overload in the genesis of cardiac arrhythmias. J Cardiovasc Electrophysiol 1997;8:700–721.

[13] Murphy E, Eisner D. Regulation of intracellular and mitochondiral sodium in health and disease. Circ Res 2009; 104:292–303.

[14] Pelzmann B, Schaffer P, Bernhart E, Lang P, Machler H, Rigler B, Koidl B. L-type calcium current in human ventricular myocytes at a physiological temperature from children with tetralogy of fallot. Cardiovasc Res 1998;38:424–432.

[15] Li GR, Yang B, Feng J, Bosch RF, Carrier M, Nattel S. Transmembrane ica contributes to rate-dependent changes of action potentials in human ventricular myocytes. Am J Physiol Heart Circ Physiol 1999;276:H98–106.

[16] Magyar J, Iost N, Körtvély Á, Bányász T, Virág L, Szigligeti P, Varró A, Opincariu M, Szécsi J, Papp JG, Nánási PP. Effects of endothelin-1 on calcium and potassium currents in undiseased human ventricular myocytes. Pflugers Arch 2000;441:144–149.

[17] Jost N, Varro A, Szuts V, Kovacs PP, Seprényi G, Biliczki P, Lengyel C, Prorok J, Bitay M, Ördög B, Szabad J, Varga-Orvos Z, Puskas L, Cotella D, Papp JG, Virag L, Nattel S. Molecular basis of repolarization reserve differences between dogs and man. Circ 2008;118 Suppl-2:S342 (abstract).

[18] Franz MR, Swerdlow CD, Liem LB, Schaefer J. Cycle length dependence of human action potential duration in vivo. Am Clin Inves 1988;82:972–979.

Address for correspondence:

Jesús Carro Fernández
Campus Río Ebro. Edificio I+D+i. Laboratorio 5.1.02
C/ Mariano Esquilor s/n. CP: 50.018 - Zaragoza, SPAIN.
jcarro@unizar.es

Appendix C

Abbreviations

- ADP: Adenosine Diphosphate
- AP: Action Potential
- APD: Action Potential Duration
- APDR: Action Potential Duration Restitution
- ATP: Adenosine Triphosphate
- CI: Coupling Interval
- CL: Cycle Length
- CRLP: Model proposed in this work
- CV: Conduction Velocity
- CVD: Cardiovascular Disease
- DI: Diastolic Interval
- ECG: Electrocardiogram
- EGM: Electrogram
- ERP: Effective Refractory Period
- EU: European Union
- GPB: Grandi et al. (2010) model
- ODE: Ordinary Differential Equations
- PDE: Partial Differential Equations
- SCD: Sudden Cardiac Death
- TNNP04: ten Tusscher et al. (2004) model
- TP06: ten Tusscher and Panfilov (2006) model
- VF: Ventricular Fibrilation
- VT: Ventricular Tachycardia

Universidad
Zaragoza
1542
Communications Technology Group
Group of Structural Mechanics and Material Modeling